REPORT NO. DOT-TSC-RSPA-78-23

A COMPARATIVE STUDY OF THE RIDE QUALITY OF TRACV SUSPENSION ALTERNATIVES

R.A. Luhrs
L.M. Sweet
H.C. Curtiss, Jr.

Princeton University
Department of Mechanical and Aerospace Engineering
Princeton NJ 08540

JUNE 1979
INTERIM REPORT

DOCUMENT IS AVAILABLE TO THE PUBLIC
THROUGH THE NATIONAL TECHNICAL
INFORMATION SERVICE, SPRINGFIELD,
VIRGINIA 22161

Prepared for

U.S. DEPARTMENT OF TRANSPORTATION
RESEARCH AND SPECIAL PROGRAMS ADMINISTRATION
Office of Transportation Programs Bureau
Washington DC 20590

Technical Report Documentation Page

1. Report No.	2. Government Accession No.	3. Recipient's Catalog No.
DOT-TSC-RSPA-78-23		

4. Title and Subtitle	5. Report Date
A COMPARATIVE STUDY OF THE RIDE QUALITY OF TRACV SUSPENSION ALTERNATIVES	June 1979
	6. Performing Organization Code
7. Author(s)	8. Performing Organization Report No.
R.A. Luhrs, L.M. Sweet, and H.C. Curtiss, Jr.	DOT-TSC-RSPA-78-23
9. Performing Organization Name and Address	10. Work Unit No. (TRAIS)
Princeton University* Department of Mechanical & Aerospace Engineering Princeton, NJ 08540	RS906/R9505
	11. Contract or Grant No.
	DOT-TSC-682
12. Sponsoring Agency Name and Address	13. Type of Report and Period Covered
U.S. Department of Transportation Research and Special Programs Administration Office of Transportation Programs Bureau Washington DC 20590	Interim Report Sept. 1976 - Sept. 1977
	14. Sponsoring Agency Code

15. Supplementary Notes

*Under contract to: U.S. Department of Transportation
Research and Special Programs Administration
Transportation Systems Center
Cambridge MA 02142

16. Abstract

A linearized model of the pitch-heave dynamics of a Tracked Ram Air Cushion Vehicle is presented. This model is based on aerodynamic theory which has been verified by wind tunnel and towed model experiments. The vehicle is assumed to be equipped with two controls which can be configured to provide various suspension system characteristics. The ride qualities and dynamic motions of the rigid vehicle moving over a guideway described by roughness characteristics typical of highways is examined in terms of the rms values of the vertical acceleration in the foremost and rearmost seats in the passenger cabin and the gap variations at the leading and trailing edges of the vehicle. The improvement in ride qualities and dynamic behavior which can be obtained by passive and active suspension systems is examined and discussed. Optimal regulator theory is employed to design the active suspension system. The predicted rms values of the vertical acceleration in the one-third octave frequency bands are compared with the vertical ISO Specification. It is shown that marked improvements in the ride qualities can be obtained with either the passive or active suspension systems.

17. Key Words	18. Distribution Statement
Ram Air Cushion Vehicle Dynamics Tracked Ram Air Cushion	DOCUMENT IS AVAILABLE TO THE PUBLIC THROUGH THE NATIONAL TECHNICAL INFORMATION SERVICE, SPRINGFIELD, VIRGINIA 22161

19. Security Classif. (of this report)	20. Security Classif. (of this page)	21. No. of Pages	22. Price
Unclassified	Unclassified	136	

Form DOT F 1700.7 (8-72) Reproduction of completed page authorized

PREFACE

Research into the possibility of using aerodynamic lift for application to ground transportation vehicles has been carried out at a very low level for approximately 12 years. This has been limited to simple analytical investigations and small-scale experiments. During this time, the concept has gone through considerable evolution beginning with a simple body designed to travel through a tube and reaching the stage of a vehicle traveling in an open guideway with flexibly mounted winglets.

In 1973, a system definition study was completed which described the characteristics of a full scale system. The so-called Tracked Ram Air Cushion Vehicle (TRACV) requires relatively little energy for suspension and has a potential for low guideway cost due to the large average air gap.

This report is the second in a series describing research conducted at Princeton University on the TRACV. Previous reports have focused on establishing stability coefficients; the present report uses these in an analysis which predicts dynamic performance of various designs.

Funding for this research was provided through the Transportation Advanced Research Program (TARP). This program was originally a part of the Office of the Secretary (OST) but has been transferred to the newly formed Research and Special Programs Administration (RSPA). Technical direction for the effort was provided by the Advanced Systems Office of the Transportation Systems Center.

TABLE OF CONTENTS

LIST OF ILLUSTRATIONS (cont.)

LIST OF TABLES

H_1, H_2, H_3	matrices (Table D-I)
HM	winglet hinge moment about axis indicated by subscript, ft-lb
K	spring matrix (Table D-I), winglet spring characteristic, as indicated by subscript, ft-lb/rad (Eq. 19)
k_y	radius of gyration of the vehicle in pitch, ft
L	lift, lb
M	vehicle pitching moment about center of gravity, positive nose up, performance index transformation matrix (Table D-V)
m	vehicle mass, slug
R	solution of steady-state matrix Ricatti equation
r_o	nondimensional parameter, $r_o = \frac{2\delta}{W\alpha}$
r_1	nondimensional parameter, $r_1 = -\frac{2c\ \theta w}{W\ \alpha}$
S	vehicle surface area, S = Wc
s	Laplace operator
t	time
U	vehicle trim velocity, U = 300 fps
u	control vector
W	vehicle width including winglets, W = 15 ft
W_w	winglet width or span, W_w = 2.5 ft
w	noise or disturbance vector
x	distance along vehicle from leading edge, ft, state variable vector as indicated by subscript (Appendix D)
x_{cg}	distance of vehicle center of gravity from leading edge, ft (x_{cg} = 60 ft)

ρ	density of air, $\rho = 0.00238$ slugs/ft^3
τ_A	aerodynamic time scale, $\tau_A = \frac{c}{U} = 0.5$ sec
τ_D	dynamic time scale, $\tau_D = \left(\frac{c\, C_{L_o}}{g}\right)^{\frac{1}{2}} = 1.456$ sec
Φ	power spectral density of quantity indicated by subscript

Subscripts

c.p.	center of pressure
g	guideway characteristic
L.E.	leading edge
n	variable index
r	vehicle coordinate measured relative to guideway
T.E.	trailing edge
v	vehicle coordinate measured relative to inertial frame
w	of the winglet
o	initial value; steady-state value
ga	apparent guideway characteristic
$(\ )_1$	winglet characteristic about longitudinal axis
$(\ )_2$	winglet characteristic about lateral axis
$(\ )_{LE}$	measured at leading edge
$(\ )_{TE}$	measured at trailing edge
$(\ )_A$	aerodynamic force of moment due to vehicle motion perturbation
$(\ )_C$	aerodynamic force of moment due to control deflection

1. INTRODUCTION

Reliable and inexpensive high-speed intercity transportation is receiving increasing attention as the cost of operating automobiles continues to soar. Present modes, however, face time and convenience problems which the car does not. Aircraft are capable of cruising at great speed, but the time lost on the ground getting into and out of airports can be many times the enroute time on short and medium distance runs. In addition, due to space requirements, airports usually cannot be located in or near the center of cities. Trains do not face the same requirements; their stations are often in the heart of the business district of town. But while trains have terminal convenience, they often have as little as one-tenth the cruise speed of aircraft.

The most convenient form of mass transit would combine the better half of each of these, giving both high speed and terminal convenience to the vehicle. High speed ground transportation can provide this combination once the issues of public safety and construction problems are resolved. Several schemes have been advanced and the most promising fall into three major categories: high-speed rail, magnetic levitation (mag-lev), and air cushion vehicles. Each of the classes has varying subtypes with advantages and drawbacks.

The high-speed rail concept utilizes improved vehicles and rails. However, high speed increases the consequences of the ever-present derailment threat, and road maintenance is particularly costly if freight must also move on the high quality rails. Magnetically levitated vehicles

3) a vehicle with moveable control surfaces whose motions are determined by suitable feedback of the motion variables. The basic performance of the three systems is examined in terms of vertical acceleration and adequate clearance between the vehicle and the guideway.

T. M. Barrows and S. E. Widnall (1970) presented an analysis which laid the groundwork for predicting the aerodynamic characteristics of a "ram wing" vehicle. Expressions for heave and pitch forces due to ground disturbances are developed and the ride quality of the heave-only constrained vehicle is discussed.

W. E. Fraize and T. M. Barrows (1973) conducted a system definition study which hypothesized a 154-foot long vehicle with a one hundred passenger capacity. This extensive study defined all aspects of a full-scale system and studied feasibility and basic dynamics. Appendix C of this reference discusses the heave dynamics of a TRACV with winglet rotation for heave control and performs a body heave-winglet dynamics analysis which was later found to contain some errors. Earlier in 1973, Barrows presented a paper which shows that almost any body natural frequency and damping ratio can be achieved in a suspended TRACV and discusses some active control concepts in TRACV suspension.

P. V. Aidala (1974) studied the lateral stability of the TRACV and determined stability derivatives. His report also compares lift forces with the numerical predictions of a one-dimensional flow mass conservation theory given by Boccardoro (1973), and shows that lateral and longitudinal forces may be considered independent.

variations at the leading and trailing edges of the winglets will tend to be limiting values. The reason for the small winglet gap is that the winglets essentially act as a pressure seal to make the flow approximately two-dimensional under the vehicle resulting in favorable lift/drag ratios. Because of this small clearance at the winglet lip compared to the clearance at the lower surface of the vehicle, the lift variation with height or heave is primarily due to winglet gap variation. The strong dependence of lift on winglet gap implies that the ride characteristics can be controlled by allowing the winglets to rotate with respect to the hull.

This report first discusses the aerodynamic model used to predict the stability derivatives, and then develops the influence of control surface deflection on the aerodynamics. The model for guideway roughness is described along with the treatment of short-wavelength guideway disturbances.

The dynamics of the rigid vehicle are discussed. The rms vertical acceleration in one-third octave frequency bands is compared to the ISO standard, and rms values of acceleration and winglet gap variation are presented. These are the measures used in this study to evaluate ride quality.

Next, the passively suspended vehicle model is developed. Springs and dampers are attached between the winglets and the hull. The values for the spring and damper constants are selected according to a criterion based on acceleration, gap variation, and winglet deflection. The procedure used is a four-variable gradient search performed on a digital computer.

The model for the active suspension system is then described. Linear optimal regulator theory is applied to determine optimal feedback gains

2. VEHICLE EQUATIONS OF MOTION

Since the TRACV is supported by aerodynamic forces, a mathematical model describing its dynamic motions is similar in some respect to that of an aircraft, consequently the terminology of aircraft stability and control is convenient. The longitudinal equations of motion are uncoupled from the lateral/directional equations as a consequence of vehicle symmetry. It is assumed that the dynamic motions that are of primary interest in determining the ride qualities are the higher frequency modes which take place at constant velocity. Thus, only the modes of motion which correspond to the aircraft short period are included in the analysis and the phugoid is neglected. The phugoid may be of importance, however a more detailed vehicle description including the nature of the propulsion systems is necessary in order to include the horizontal velocity as a degree of freedom. It is unlikely that significant vertical accleration would be associated with this mode. Consequently only the lift and pitching moment equations of motion are required to describe the vehicle dynamics. These two equations of motion describe the pitch-heave dynamics of the vehicle and are expressed in terms of lift and pitching moment coefficient variations. Since the TRACV operates in ground effect, the lift and pitching moment will depend upon the displacement of the vehicle with respect to the ground as well as the velocities and consequently the constant velocity dynamics will be fourth order in contrast to an aircraft where the constant velocity approximation leads to a second order system. The equations of motion are formulated in nondimensional terms since there are no specific

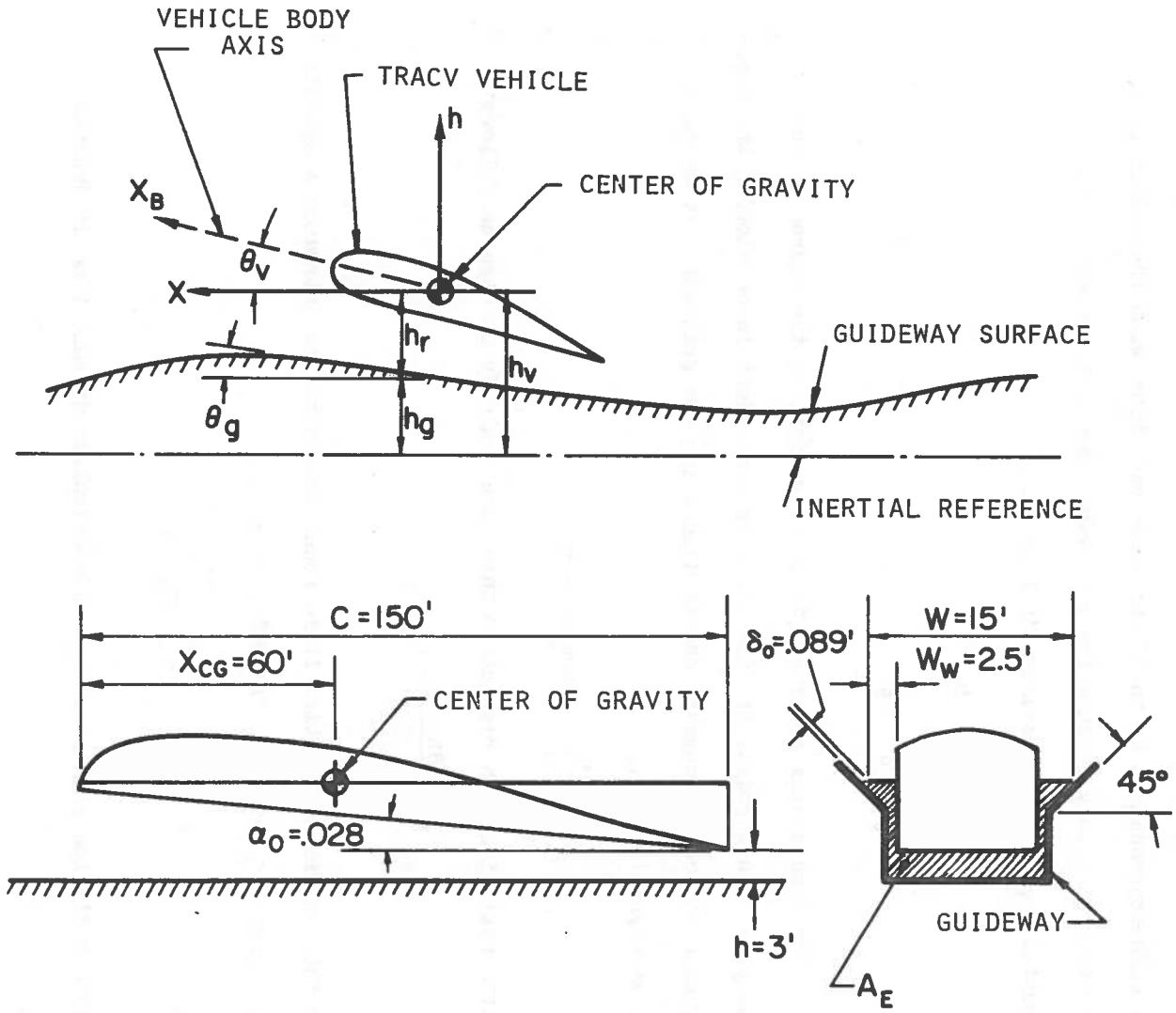

FIGURE 1. VEHICLE GEOMETRY, COORDINATE SYSTEM AND MOTION VARIABLES

$$h' = \frac{dh}{d(\frac{t}{\tau_D})} = \tau_D \dot{h} .$$

Therefore, in the following, other quantities such as frequencies and power spectral densities are denoted as dimensionless in time by the following notation,

$$\hat{\omega} = \tau_A \omega \qquad \hat{\Phi} = \frac{1}{\tau_A} \Phi$$

$$\tilde{\omega} = \tau_D \omega \qquad \tilde{\Phi} = \frac{1}{\tau_D} \Phi .$$

2.2 Aerodynamic Parameters

The aerodynamic characteristics of the vehicle are described in terms of the lift and pitching moment coefficients. It can be shown that these coefficients may be expressed as functions of three dimensionless parameters: $\bar{\alpha}$, r_o, r_1 in steady flight. The dependence of the lift and pitching moment coefficients on $\bar{\alpha}$ and r_o is developed by Curtiss and Putman (1977) where it is also shown that the theory employed agrees well with experiment. The dependence on vehicle attitude given by the parameter r_1 is based on unpublished work by Curtiss. These three parameters can be viewed as ratios of various areas related to the geometry of the model and guideway. Analytical expressions for lift and pitching moment were developed using a one-dimensional flow model which essentially employs the continuity equation with suitable boundary conditions to determine the pressures acting on the lower surface of the vehicle and consequently the lift and pitching moment.

axis and the guideway and consequently includes both vehicle pitch and winglet rotation.

Changes in vehicle height and attitude with respect to the guideway, Δh_r and θ_r as well as winglet deflections about both axes $\Delta\delta_{w_1}$ and $\Delta\delta_{w_2}$ alter these parameters and consequently change the lift and pitching moment coefficients. The following relationships are involved assuming that the initial pitch attitude of the vehicle is zero:

$$\begin{aligned} \alpha &= \alpha_o + \theta_r \\ \delta &= \delta_o + 0.707\,[\Delta h_r + W_w\,\Delta\delta_{w_1}] \\ \theta_w &= \theta_r + \Delta\delta_{w_2} \\ A_E &= A_{E_o} + W\,\Delta h_r \end{aligned} \qquad (2)$$

where the subscript o refers to the equilibrium or trim value.

The dependence of the lift and pitching moment coefficients on vertical velocity and pitch rate must also be included for a complete description of the vehicle aerodynamics. The rate dependent terms are given in Appendix B.

2.3 Vehicle Controls

Like other aerodynamic vehicles, the TRACV may require surfaces to exert forces and moments on the vehicle to control the flight of the

vehicle as well as the ride qualities. Since two motion degrees-of-freedom are involved, two controls are desirable. It would be convenient from a control standpoint if the controls selected provided lift and pitching moment variations independently. Although a variety of control configurations are possible, a configuration which provides independent control inputs and is simple and effective is a two-degree-of-freedom winglet rotation. One control is rotation of the winglets about an axis parallel to the vehicle longitudinal axis designated δ_{w_1}; the second is a rotation of the winglet about an axis perpendicular to the longitudinal axis of the vehicle, at the center of gravity of the vehicle, designated δ_{w_2}, as in Figure 2. The best method for producing δ_{w_2} has not been determined. One simple concept for doing this is to provide torsional flexibility in each winglet, which would allow them to twist such that the tips assume a deflection δ_{w_2} as shown.

2.4 Equations of Motion

A linearized small perturbation approach is employed to analyze the dynamics of the TRACV. Since large dynamic motions while cruising necessarily imply poor ride quality, as well as frequent contact with the guideway, large motions must be prevented by the natural dynamics of the vehicle or a suitable feedback control or a suspension design. Therefore, it is assumed that the lift and pitching moment variation may be described by a Taylor series including only first order terms. As a consequence of linearization

A complete development of these terms is also presented in Appendix B. It is assumed that the effects of winglet motion rate ($\dot{\delta}_{w_1}$ and $\dot{\delta}_{w_2}$) on vehicle aerodynamics is negligible. This assumption is consistant with the aerodynamic model employed for the overall vehicle aerodynamics. Winglet rate effects would be important only when the winglets are free with respect to the vehicle and when that case is examined here, mechanical dampers are employed which give terms of similar form. Consequently winglet aerodynamic damping would have an influence on the actual damper values.

The resulting equations of motion are a coupled pair of second order equations with the motion variables $\dot{\bar{h}}$, $\bar{h}$, $\dot{\theta}$ and θ, and the control variables δ_{w_1} and δ_{w_2}. The aerodynamic forces and moments acting on the vehicle are dependent upon the motion of the vehicle with respect to the guideway ($\bar{h}_r$, θ_r). The perturbation equations of motion for the vehicle are therefore written as,

$$\frac{m}{\frac{1}{2}\rho U^2 S}\ddot{h}_v = \frac{\partial C_L}{\partial \dot{\bar{h}}}\Delta\dot{\bar{h}}_r + \frac{\partial C_L}{\partial \dot{\theta}}\Delta\dot{\theta}_r + \frac{\partial C_L}{\partial \bar{h}}\Delta\bar{h}_r + \frac{\partial C_L}{\partial \theta}\Delta\theta_r + \frac{\partial C_L}{\partial \delta_{w_1}}\Delta\delta_{w_1} + \frac{\partial C_L}{\partial \delta_{w_2}}\Delta\delta_{w_2}$$

$$\frac{I_y}{\frac{1}{2}\rho U^2 Sc}\ddot{\theta}_v = \frac{\partial C_M}{\partial \dot{\bar{h}}}\Delta\dot{\bar{h}}_r + \frac{\partial C_M}{\partial \bar{h}}\Delta\bar{h}_r + \frac{\partial C_M}{\partial \theta}\Delta\theta_r + \frac{\partial C_M}{\partial \delta_{w_1}}\Delta\delta_{w_1} + \frac{\partial C_M}{\partial \delta_{w_2}}\Delta\delta_{w_2} \qquad (5)$$

in the frequency domain as experienced by a vehicle travelling over the roadway at constant velocity U is

$$\Phi_{h_g}(s) = -\frac{AU}{s^2} \tag{7}$$

where A is a surface roughness parameter (Hedrick, Billington, and Dreesbach, 1974). For a smooth highway,

$$A = 1.27\,\pi \times 10^{-6}\ \text{ft.}$$

is a typical value. This value is taken to be characteristic of the guideway. As a design specification for a TRACV guideway, this would not require strict construction tolerances driving the construction costs above practical limits.

It is convenient for purposes of this analysis to be able to express this input to the vehicle as white noise which has been filtered. With white noise as an input, standard methods for optimal regulator design such as found in Bryson and Ho (1969) may be directly applied. Nondimensionalizing the roughness height by the vehicle chord, c, and the time scale by the dynamic time τ_D equation (7) becomes,

$$\tilde{\Phi}_{\tilde{h}_g}(\tilde{s}) = \frac{\Phi_{h_g}(\tilde{s})}{c^2 \tau_D} = -\frac{(2\mu)^{\frac{1}{2}} \bar{A}}{\tilde{s}^2} \tag{8}$$

If white noise is passed through a filter with transfer characteristics $\tilde{G}_1(\tilde{s})$ then the output power spectral density is

$$\tilde{\Phi}_{\tilde{h}_g}(\tilde{s}) = |\tilde{G}_1|^2 \tilde{\Phi}_{\tilde{n}}(\tilde{s}) \tag{9}$$

The power spectral density of the dimensionless white noise $\tilde{\Phi}_{\tilde{n}}(\tilde{s})$ is taken equal to 1, such that the filter characteristic given by equations (8) and

employed, that is, $\hat{\omega} = \frac{\omega c}{U}$ is small. Since $\omega = \frac{2\pi U}{\lambda}$, $\hat{\omega} = 2\pi \frac{c}{\lambda}$ so that there are consistant assumptions for the aerodynamics. Rather than extending the aerodynamic theory to include short wavelengths and unsteady effects, it is assumed that the variables which primarily affect the dynamic motions of the vehicle are the averages of the guideway variables over the length of the vehicle. Wavelength disturbances which are short compared to the length of the vehicle are filtered by modifying the guideway description rather than the aerodynamic model. The approach is developed in detail in Appendix C (Ribich, Captain, and Richardson, 1967). The effect of averaging guideway variables is to attenuate the guideway height spectrum. The relationship between the apparent height and the actual height is

$$\left| \frac{h_{g_a}(\hat{\omega})}{h_g(\hat{\omega})} \right| = \left| \frac{\sin \frac{\hat{\omega}}{2}}{\frac{\hat{\omega}}{2}} \right| \tag{11}$$

The magnitude of this attenuation can be closely approximated by a second order filter as shown in Appendix C. A second order filter was chosen because it had sufficient attenuation with frequency to insure that no infinite accelerations are predicted for the vehicle as would be the case with a first order model, although it slightly overestimates the attenuation given by equation (11). This equivalent filter has the transfer function in dynamic time of

$$G_p(\tilde{s}) = \frac{h_{g_a}(\tilde{s})}{h_g(\tilde{s})} = \frac{1}{(1 + \frac{0.24}{(2\mu)^{\frac{1}{2}}}\tilde{s})(1 + \frac{0.36}{(2\mu)^{\frac{1}{2}}}\tilde{s})} \tag{11a}$$

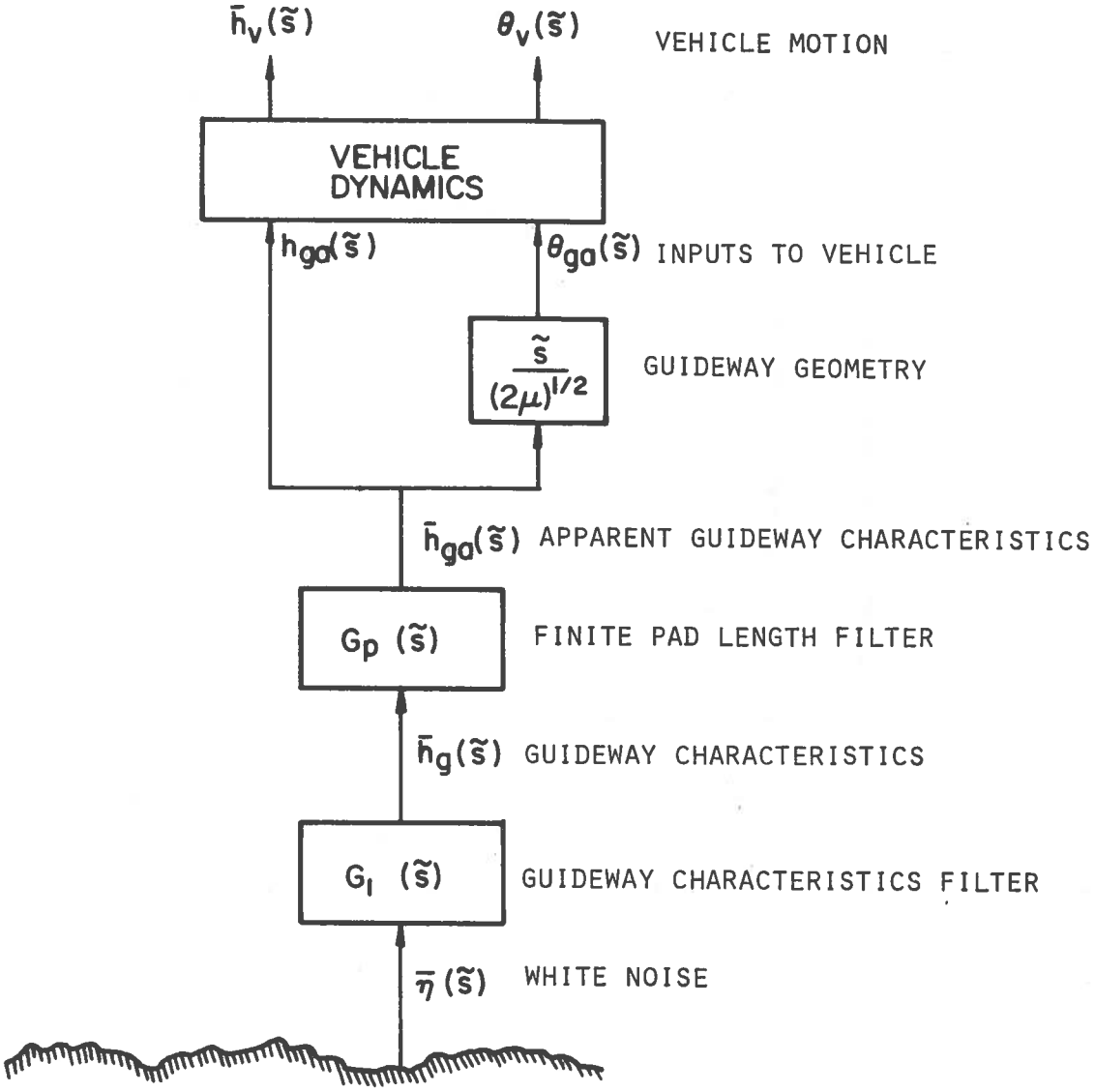

FIGURE 3. BLOCK DIAGRAM ILLUSTRATING MODELLING OF GUIDEWAY INPUTS TO VEHICLE

TABLE I

VEHICLE CHARACTERISTICS, EIGENVALUES AND EIGENVECTORS FOR RIGID VEHICLE

A.) Vehicle Geometric and Mass Characteristics

c =	150 ft.	W_w =	2.5 ft.
W =	15 ft.	δ =	0.089 ft.
U =	300 fps	h_{TE} =	3 ft.
α_o =	0.028 rad.	GW =	110,000 lbs.
		I_y =	7.2×10^6 slug-ft^2

B.) Dimensionless Characteristics

C_{L_o} =	0.455	r_o =	0.5
τ_A =	0.5	$\bar{\alpha}$ =	1.4
τ_D =	1.456	$\bar{k}_y$ =	0.306
$\bar{x}_{cg}$ =	0.40	μ =	4.24

C.) Eigenvalues, Eigenvectors

1.) Non-dimensional dynamic time

High Frequency

$- 3.02 \pm 13.11\ i$ $\qquad \frac{\bar{h}_r}{\theta_r} = 3.30\ e^{59.2^o i}$

Low Frequency

$- 0.686 \pm 8.78\ i$ $\qquad \frac{\bar{h}_r}{\theta_r} = 0.54\ e^{-3.37^o i}$

2.) Real Time

High Frequency

$P = 0.70$ seconds, $\zeta = 0.24$

Low Frequency

$P = 1.04$ seconds, $\zeta = 0.08$

height variable has been nondimensionalized by the length of the vehicle, this value implies that in this mode of motion the vehicle has an effective center of rotation at about the 94 percent chord position, almost at the trailing edge.

On the other hand, for the high frequency mode the heave motion is approximately sixty degrees out of phase with pitch and the amplitude ratio is six times larger than that of the low frequency mode. This result implies that the high frequency mode is primarily a heaving motion. The pitching motion is small and will not contribute significantly to the vertical acceleration in contrast to the low frequency mode. This effect is apparent in the spectral density plots which follow, particularly if one remembers that part of the high frequency reduction at ninety percent chord is due to the reduced reinforcement of the nearby low frequency mode.

Figure 1 shows a time history of the rigid vehicle response to an initial condition disturbance. It can be seen that after a short time interval, the transient response is dominated by the high frequency lightly damped mode. The phase relationship indicated by the eigenvector for this mode can be clearly seen. This mode characteristic as noted above, indicates that forward locations in the vehicle will experience the roughest ride.

3.2 Spectral Density of the Response and Ride Quality

Table D-II gives the A and D matrices for the rigid vehicle. Since there are no control motions (rigid winglets), the B matrix is not involved. The vehicle transfer functions, which represent the response of the vehicle to the white noise input are calculated. Since the power spectral density of the dimensionless white noise disturbance $\bar{\eta}(\tilde{t})$ is one, the magnitude squared of

transfer functions give the power spectral density of the response as a function of frequency. The spectral densities of interest here are those associated with vehicle acceleration, specifically the vertical acceleration spectra. To give an indication of the ride qualities at various locations in the vehicle, the vertical acceleration spectra are shown at the center of gravity of the vehicle (40 percent chord) and near the trailing edge (90 percent chord) in Figure 5. The vertical acceleration at any longitudinal position on the vehicle is found by a suitable linear combination of the vertical and the pitch acceleration. The results can then be compared with various ride quality standards to evaluate the ride qualities of the vehicle.

In order to compare the acceleration spectral densities with ride quality specifications it is desirable to present the results in dimensional form. The power spectrum which is calculated directly from the equations of motion is dimensionless and is related to the dimensional spectra, $\Phi_{\ddot{h}}(\omega)$ by,

$$\tilde{\Phi}_{\tilde{h}''_V}(\tilde{\omega}) = \frac{\tau_D^3}{c^2}\, \Phi_{\ddot{h}_V}(\omega) \tag{15}$$

The power spectrum which is presented in Figure 5 is normalized by the acceleration of gravity, g. Using the notation A_H to denote heave acceleration normalized by g,

$$\tilde{\Phi}_{A_H}(\tilde{\omega}) = \frac{1}{g^2 \tau_D}\, \Phi_{\ddot{h}_V}(\omega) \tag{16}$$

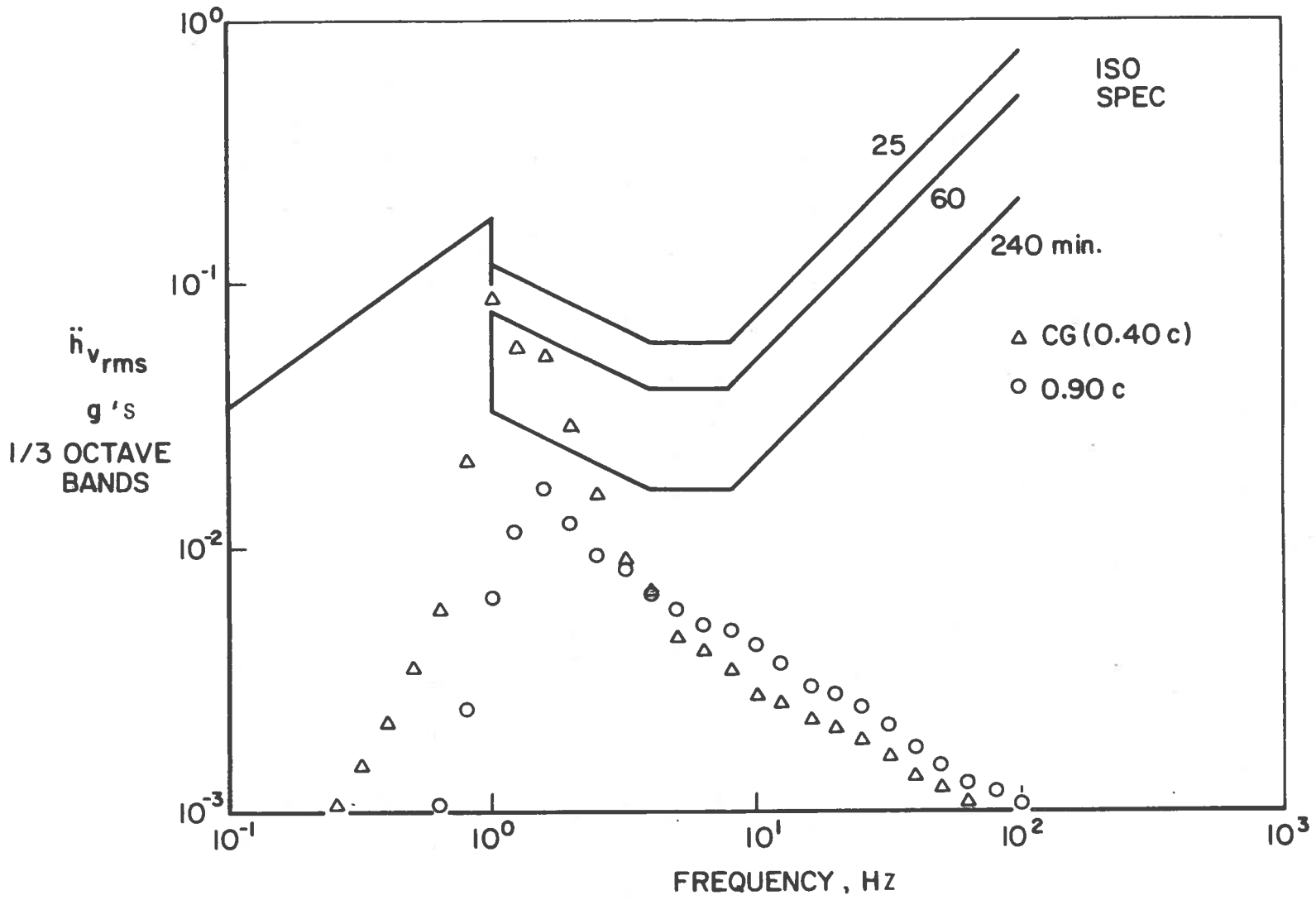

FIGURE 6. COMPARISON OF RMS VERTICAL ACCELERATION IN ONE-THIRD OCTAVE BANDS WITH ISO SPECIFICATIONS. RIGID VEHICLE

steady-state value of about one inch. These values indicate that the vehicle is likely to spend much of its time in contact with the guideway, or simply put, it will "bottom out" frequently, particularly at the front, primarily because of the influence of the very lightly damped low frequency mode. The reader should remember that these numbers are the result of a linear model and while they should be reasonable as estimates of the small perturbation motion, the actual motion of the vehicle on a rough guideway would in fact be quite different owing to the fact that the guideway would be contacted by the vehicle frequently.

The conclusion to be drawn from this rigid case analysis is that from all measures the ride quality of the rigid vehicle is unacceptable. There are frequencies in all seat locations where the accelerations are uncomfortable. The overall ride is rough, and the vehicle tends frequently to strike the guideway. The vehicle has one oscillatory mode which is very lightly damped with a period of about one second which is in a large measure responsible for these problems. The high frequency mode is nearby and aggravates the ride quality dynamics. It is readily apparent that some form of suspension or control is necessary if the TRACV is to be implemented. The Sections that follow explore this possibility. Both passive and active suspension systems are examined and compared to determine the degree of improvement that can be achieved.

addition, the uncoupled natural frequencies of the winglet will be high compared to the rigid modes of the vehicle. Winglet damping is included however, so that two first order equations are added to the equations of motion of the vehicle, one for each degree-of-freedom of the winglets. The motions of the winglets $\Delta\delta_{w_1}$ and $\Delta\delta_{w_2}$ are considered state variables. Values of spring and damper constants which give the best performance as determined by minimizing a cost function are determined as explained below and then the ride quality is examined.

A moment balance equation is developed for each winglet motion assuming small perturbations. The aerodynamic moment acting on the winglet is assumed to be proportional to the pressure distribution on the lower surface of the vehicle and is a function of the motion and control variables,

$$B_1 \frac{d\Delta\delta_{w_1}}{dt} + K_1 \Delta\delta_{w_1} = HM_1 \left(D\bar{h}_r, D\theta_r, \bar{h}_r, \theta_r, \delta_{w_1}, \delta_{w_2}\right)$$

$$B_2 \frac{d\Delta\delta_{w_2}}{dt} + K_2 \Delta\delta_{w_2} = HM_2 \left(D\bar{h}_r, D\theta_r, \bar{h}_r, \theta_r, \delta_{w_1}, \delta_{w_2}\right) \qquad (19)$$

In the above equations, HM_1 and HM_2 refer to the hinge moment around the longitudinal and lateral winglet axes, respectively. K_1, K_2, B_1 and B_2 are the spring and damper characteristics about the two winglet rotation axes to be determined from the ride quality considerations as explained below. It has been assumed that the winglet is mass balanced about each of its hinge axes. The hinge moment of the winglet about its longitudinal axis is proportional to vehicle lift, since the pressure distribution which produces the vehicle

winglet rotation axis due to lift acting at the center of gravity, and the second relates the effect of the longitudinal pressure distribution which produces the aerodynamic pitching moment about the center of gravity. The winglet rotational axis is taken to be at the center of gravity of the vehicle such that $\bar{x}_{cg} = \bar{x}_{cr}$, so that the first term vanishes. Therefore,

$$HM_2 = \frac{A_w}{2S} M$$

Nondimensionalizing,

$$HM_2 = \frac{A_w \rho U^2 c}{4} C_M \; ; \; HM_2 = h_m C_M$$

Consequently, the hinge moment derivatives about the lateral axis are directly related to the pitching moment derivatives on the vehicle. Note however that the dimensionless pitching moment derivatives include the radius of gyration of the vehicle such that

$$\frac{\partial HM_2}{\partial(\;)} = h_m \bar{k}_y^2 \, C_{M_{(\;)}}$$

Expanding the right hand side of equations (19) in a Taylor series and nondimensionalizing the winglet equations of motion are:

$$\begin{aligned} b_1 \Delta\delta_{w_1}' &= \frac{h_m \bar{y}_{cp}}{(2\mu)^{\frac{1}{2}}} C_{L_{D\bar{h}}} \Delta\bar{h}_r' + \frac{h_m \bar{y}_{cp}}{(2\mu)^{\frac{1}{2}}} C_{L_{D\theta}} \Delta\theta_r' + h_m \bar{y}_{cp} C_{L_{\bar{h}}} \Delta\bar{h}_r \\ &\quad + C_{L_\theta} \Delta\theta_r + (h_m \bar{y}_{cp} C_{L_{\delta_{w_1}}} - K_1) \Delta\delta_{w_1} + h_m \bar{y}_{cp} C_{L_{\delta_{w_2}}} \Delta\delta_{w_2} \end{aligned} \tag{20}$$

$$\begin{aligned} b_2 \Delta\delta_{w_2}' &= \frac{h_m \bar{k}_y^2}{(2\mu)^{\frac{1}{2}}} C_{M_{D\bar{h}}} \Delta\bar{h}_r' + \frac{h_m \bar{k}_y^2}{(2\mu)^{\frac{1}{2}}} C_{M_{D\theta}} \Delta\theta_r' + h_m \bar{k}_y^2 C_{M_{\bar{h}}} \Delta\bar{h}_r \\ &\quad + C_{M_\theta} \Delta\theta_r + h_m \bar{k}_y^2 C_{M_{\delta_{w_1}}} \Delta\delta_{w_1} + (h_m \bar{k}_y^2 C_{M_{\delta_{w_2}}} - K_2) \Delta\delta_{w_2} \, . \end{aligned}$$

counter, ϵ_n is the step size constant for x_n, and J is the cost function. The procedure involves finding the partial derivative of the cost function with respect to each of the four motion variables ($\bar{h}_v$, θ_v, $\bar{h}_r$, θ_r), adjusted by the corresponding ϵ_n, and use the result as a stepsize for each variable.

The cost function which was used placed a cost on six values. These values are: the rms acceleration in heave and pitch; rms gap variation fore and aft; and rms winglet deflection for both motions. These rms values were found for the given system dynamics by determining the transfer functions for each variable for the white noise input, and then calculating mean squared value of the variable. The value of x_n^{k-1} was taken as five percent larger than x_n^k rather than the actual previous value to insure that a large previous step does not adversely influence the derivatives at the present point. The cost function used is defined by

$$J = \frac{1}{2} \int_0^\infty x^T Z x \; dt \tag{23}$$

where x is a vector of the state variables and Z is a diagonal matrix of weighting constants. The values of Z were set by

$$Z(n,n) = \left| \frac{1}{x_{n_{max}}} \right|^2 \tag{24}$$

which is the inverse of the desired maximum value of each of the respective state variables. The values chosen were $\ddot{h}_{max} = 0.01$ g, $\Delta\delta = 0.33$ inches with no weighting on control deflections or pitching accelerations. These

about the longitudinal axis which must be balanced to maintain the equilibrium position of the winglet. This value is given by

$$HM_o = h_m \bar{y}_{cp} C_{L_o} = 15225 \text{ ft.-lb}$$

This set of results appears to give the optimum passive suspension for the given set of weighting coefficients. It was felt that a better suspension might be found by repeating the entire process with several sets of weighting parameters. Rather than conducting an extensive numerical search, a local search around this optimum was made using educated guessing, and no better tradeoff between vertical acceleration and gap variation could be found.

With the spring and damper constants determined, the overall model is described in state variable form with two more variables than in the rigid case; $\Delta\delta_{w_1}$ and $\Delta\delta_{w_2}$ become state variables. We now have a ninth order system which may be evaluated using the same criteria as used in the previous sections.

First we examine the eigenvalues and eigenvectors. For the passive suspension they differ significantly from the rigid case, as shown in Table II. The eigenvalues show a significant change from very low damping characterizing the rigid case and there is a marked reduction in the natural frequencies of the vehicle. For the rigid vehicle, the periods of the two motions were 0.70 seconds and 1.08 seconds; in the passive case with

flexible winglets they are 3.51 seconds and 29.2 seconds, so that the natural modes are not only slower, but they are well separated. The damping ratios of the two modes are 0.65 and 0.38 respectively. Spreading the natural frequencies apart and increasing the damping means that, on the whole, the acceleration will be much lower and more nearly uniform over the range of input frequencies.

The eigenvectors also show a marked change. The mode ratios of heave to pitch indicate that the coupling between the degrees of freedom is significantly reduced. The high frequency mode has a mode ratio, $\frac{\bar{h}_r}{\theta_r} = 212$ which is sixty-four times greater than the ratio for the rigid case, implying that the high frequency mode is entirely heave motion. For the low frequency mode, the opposite is true, the $\frac{\bar{h}_r}{\theta_r}$ ratio for the passive case is less than one-tenth that of the rigid case, that is, the low frequency mode is primarily pitch motion.

These values indicate that the free winglet motion contribution lowers the natural frequencies and decouples the degrees of freedom. The high frequency mode damping ratio has increased from the rigid case value of 0.23 to 0.65 and the low frequency ratio has improved from the rigid case 0.08 to 0.38, indicating that these winglet motions also reduce transient oscillations of the hull. Because of the very low frequency of the pitch mode, the accelerations caused by the presence of this mode are likely to be small and hence the accelerations felt by the passengers will be mostly due to

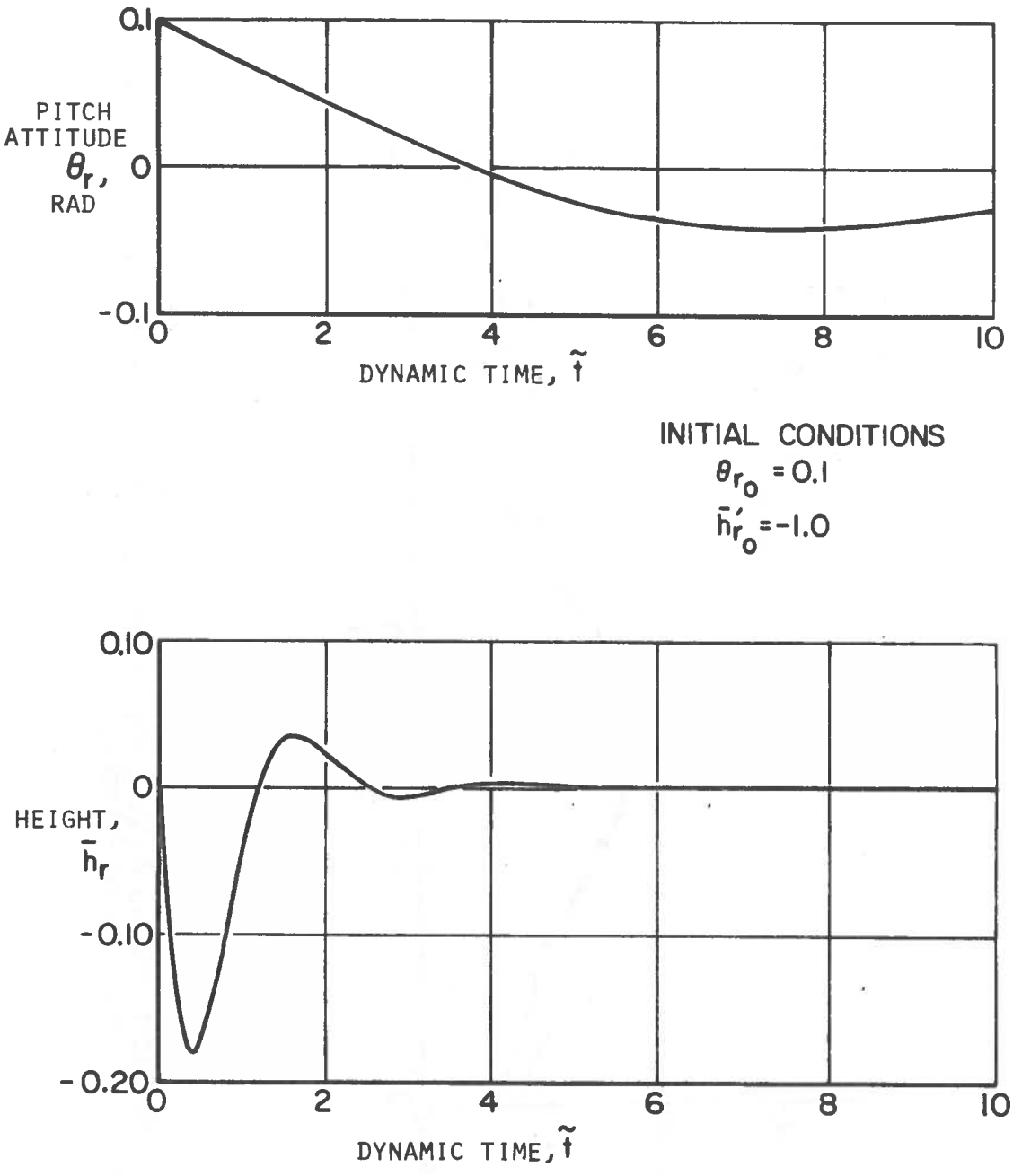

FIGURE 7. HEIGHT AND PITCH ATTITUDE TRANSIENT RESPONSE TO INIITAL CONDITION DISTURBANCE. VEHICLE WITH PASSIVE SUSPENSION

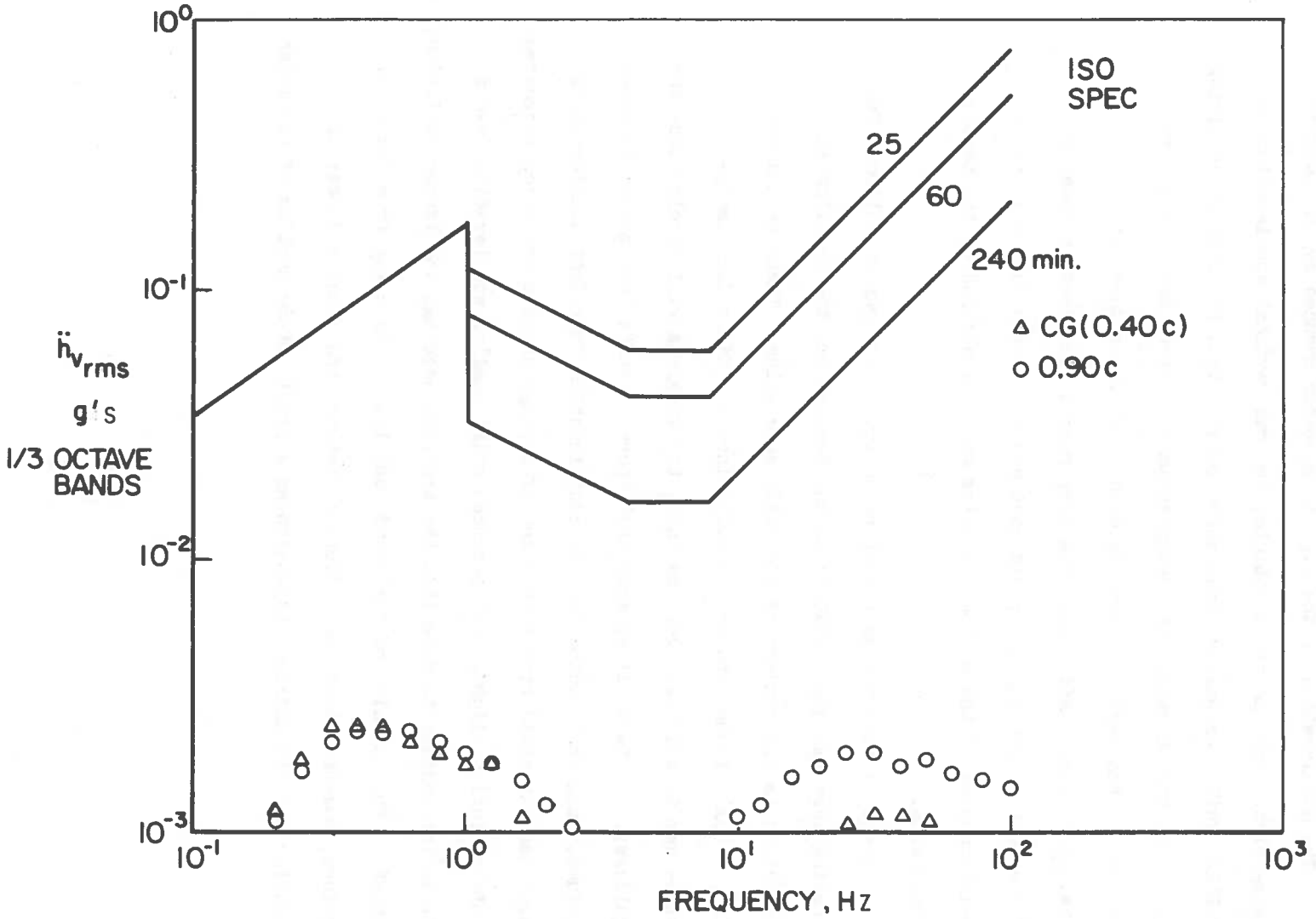

FIGURE 9. COMPARISON OF RMS VERTICAL ACCELERATION IN ONE-THIRD OCTAVE BANDS WITH ISO SPECIFICATIONS. VEHICLE WITH PASSIVE SUSPENSION

There is one other result of interest, and that is the rms deflection of the two winglet modes. For the passive suspension, rms $\Delta\delta_{w_1}$ is 0.0154 rad. and rms $\Delta\delta_{w_2}$ is 0.000534 rad. The heave control is small, varying through a typical ± 1 degree. A deflection of one degree represents a change of gap on the order of one-half inch, however, and that is significant. This result indicates that the motions of the winglet are such that the variation in guideway height are countered by similar motions of the winglet so that gap variation and heave motion of the c.g. are very small and the winglet follows the guideway. Pitch deflection of the winglet is also small, the value of 0.000534 rad. corresponds to 0.03 degree, and a gap change at either end of the vehicle of about 0.6 inches. Once again, the winglet deflection is larger than the gap variation, indicating that the winglet pitch motion is also necessary to reduce vehicle body accelerations and to prevent winglet-guideway contact.

To summarize, a passive suspension has been developed by allowing the winglets two degrees of freedom, restraining each motion with a spring and a damper. The effect of this suspension configuration (with suitably chosen springs and dampers) is to lower the frequencies of both modes as well as spreading them apart, increasing the damping, and reducing the coupling of the modes of motion. In terms of the ride quality, the passive suspension configuration is very good and represents a significant improvement over the rigid vehicle. The overall acceleration level is quite low and there are no particular "bone-jarring" frequencies. Winglet motion

4.2 Active Suspension

Active suspension implies that the winglet motion is controlled by actuators which receive signals from vehicle motion sensors. The design of the active suspension is approached using linear optimal control theory. The linear optimal control problem is solved using a performance index very similar to the one employed for the passive suspension. The form of the equations is altered slightly to accommodate the solution technique. Dynamic terms depending upon winglet angular rate and acceleration are neglected. This is equivalent to assuming that the winglet actuator dynamic response is of sufficient bandwidth to be considered infinitely fast. The method involves determining the solution of the matrix Ricatti equation and using this to find the feedback gains. Determining the feedback laws using this approach gives in a sense the best possible performance of this particular vehicle in terms of ride quality, and provides an index against which other suspension systems can be compared. After determination of the optimal feedbacks, we will proceed to analyze the ride quality along the lines of previous sections.

The active suspension model assumes a controllable dynamic system with white noise disturbance. The state equations written in matrix form are $\dot{x} = Ax + Bu + Dw$ where the A and D matrices are identical to those of the rigid vehicle model, and the B matrix is the set of derivatives of lift and moment coefficients with respect to each of the two control motions.

The optimal control problem involves finding the coefficients of a feedback matrix which produces the lowest cost function value. The cost function is selected as a function of the states of the vehicle and the control motions. The desired cost function is not chosen directly in terms of state variables. The quantities selected for the cost functions are vertical and pitch acceleration, leading and trailing edge gap variations and the two control deflections. A transformation must be performed to express the performance index as a function of actual state variables and control inputs. Let y be the vector of variables included in the cost function. x is the vector of state variables and u is the control motion. These quantities are related by a linear transformation,

$$y = M\begin{bmatrix} x \\ u \end{bmatrix} \tag{25}$$

The matrix M is given in Appendix D.

Since y is a vector with six components, x has seven and u has two, M is a six by nine matrix of constants. Let Z be a diagonal matrix of weighting factors as used previously. The cost function is expressed as follows:

$$J = \frac{1}{2}\int_{t_o}^{\infty} y^T Z\, y\, dt\,. \tag{26}$$

From equation (25)

$$J = \frac{1}{2}\int_{t_o}^{\infty} [x^T\ u^T]\, M^T \cdot Z \cdot M \begin{bmatrix} x \\ u \end{bmatrix} dt\,. \tag{27}$$

The matrix K^T is given by

$$K^T = P^{-1} (N^T + B^T R) \tag{33}$$

where R is the solution to the matrix Ricatti equation (Schultz and Melsa, 1967).

The procedure to be followed first involves determination of the linear transformation matrix M and then selection of the elements of Z, the weighting factors. Then the submatrices Q, N and P are determined from M and Z. The modified A matrix, $\tilde{A} = (A - BP^{-1}N^T)$ is calculated as well as the modified Q matrix, $\tilde{Q} = (Q - NP^{-1}N^T)$. These are substituted into the matrix Ricatti equation to determine the matrix R. The matrix Ricatti equation is

$$\tilde{A}^T R + R\tilde{A} - RBP^{-1}B^T R + \tilde{Q} = \dot{R} = 0 \tag{34}$$

$\dot{R}$ is set equal to zero since we are interested in a terminal time where $\dot{R}$ is zero. Several methods of solving equation (34) for R are available. The most convenient technique is to integrate backwards in time from the terminal condition $R(\infty) = 0$, until R is constant to within some limit, that is, until $\dot{R} \approx 0$. The optimal feedback matrix K^T is determined from (33) The closed loop system equation is given as

$$\dot{x} = (A - BK^T) x + Dw \tag{35}$$

The dynamics of the closed loop system described by equation (35) give the ride characteristics of the vehicle with the optimal controller.

Appendix E gives the appropriate logic flow diagram for the overall solution technique. The computer time involved in solving the optimal

Table IV lists the gain elements in the feedback maxtrix K^T for the optimal regulator. All of the values appear to be of reasonable size physically. It is quite difficult to interpret the role of each of these various feedback paths in improving the vehicle ride quality. This is a consequence of the fact that the pitch and heave motion of the vehicle are coupled, and the controls are coupled as well, that is, each control produces both a force and a moment. In addition, the guideway disturbances are related by the equation (6),

$$\frac{1}{U}\dot{h}_g = \theta_g \,. \tag{6}$$

The primary effect of the feedbacks which can be noted are the reduction in the vehicle height stiffness which is produced by the relative height feedback ($\bar{h}_r$) to $\Delta\delta_{w_1}$ and the reduction in the pitch stiffness produced by relative attitude feedback (θ_r) to $\Delta\delta_{w_2}$. The attitude feedback is -1.16 degrees per degree indicating that the feedback system tends to maintain the winglet nearly parallel with the guideway as is necessary to obtain a low pitch stiffness. A similar magnitude can be noted for the height feedback which is equal to - 0.565 rad per foot. The gap change caused by this feedback is given by

$$\Delta\delta_o = -\,0.707\, W_w\, \Delta\delta_{w_1}$$

with W_w = 2.5 ft. so that

$$\Delta\delta_o = 1.76\, \Delta\delta_{w_1}$$

and the feedback is

$$\Delta\delta_{w_1} = -\,0.565\, \Delta h_r$$

weighting parameters, this is the optimal solution. Table III displays the eigenvalues and eigenvectors for vehicle with controller. Compared to the rigid vehicle, the actively controlled vehicle shows improved natural dynamics. The natural frequencies are markedly reduced with periods of 6.19 seconds and 15.24 seconds for the two modes. The damping ratio for both modes is around 0.7. The damping ratios are somewhat higher than for the passive suspension, and considerably larger than for rigid vehicle.

The eigenvectors indicate that the low frequency mode ratio $\frac{\bar{h}_r}{\theta_r}$ is modified as in the case of the passive system so that this mode involves primarily pitching motion and contains very little heave motion especially when compared to the rigid case. The high frequency mode ratio $\frac{\bar{h}_r}{\theta_r}$ is almost the same as the rigid case. For the passive suspension, the high frequency mode is almost entirely heave; however, the active suspension high frequency model still contains a small amount of pitch, although still predominantly heave. Figure 10 shows a time history of the response of the vehicle with active suspension to initial conditions in θ_r and $\dot{h}_r$.

Figure 11 shows the acceleration spectral densities at the vehicle center of gravity (0.40c) and at the trailing edge (0.90c). The curves show a smooth transition from low to high frequencies and are well below the specification. There are no sharp peaks or valleys, only a very gentle rounded peak indicating the combined effect of the two modes. When compared against the corresponding figures of the other two cases, the active case proves to have the lowest vertical acceleration at any given frequency, as one might expect.

TABLE IV

FEEDBACK GAINS FOR ACTIVE SUSPENSION

1.) Nondimensional Dynamic Time

	$\Delta\delta_{w_1}$	$\Delta\delta_{w_2}$
$\bar{h}_v'$	-0.49	0.027
θ_v'	0.23	-0.022
$\bar{h}_r$	-84.75	0.127
θ_r	4.52	-1.16
$\bar{h}_{ga}'$	0.49	-0.027
θ_{ga}'	0.061	0.041
θ_{ga}	1.69	-0.0048

2.) Dimensional, Real Time

	$\Delta\delta_{w_1}$	$\Delta\delta_{w_2}$	Units
$\dot{h}_v$	-0.00474	+0.000266	rad/fps
$\dot{\theta}_v$	0.338	-0.0319	rad/rad/sec
h_r	-0.565	0.000847	rad/ft
θ_r	4.52	-1.16	rad/rad
$\dot{h}_{ga}$	0.00474	-0.000266	rad/fps
$\dot{\theta}_{ga}$	0.0885	0.0584	rad/rad/sec
θ_{ga}	1.69	-0.00477	rad/rad

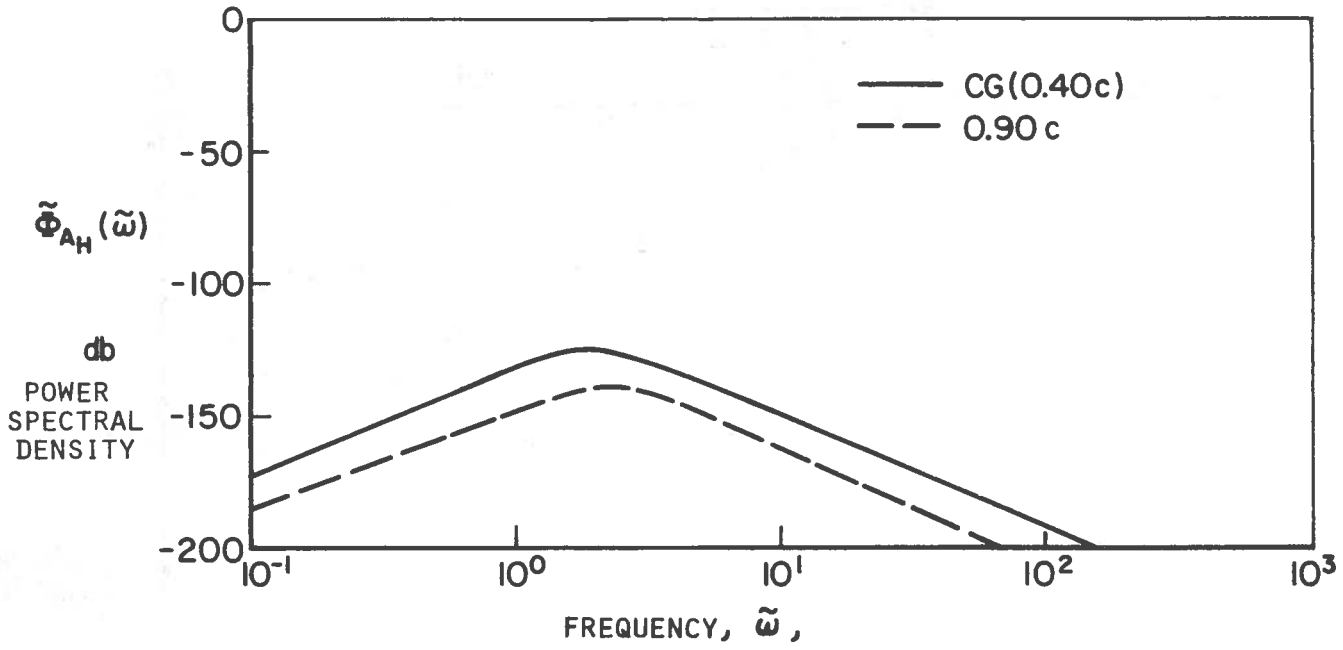

FIGURE 11. VEHICLE ACCELERATION POWER SPECTRAL DENSITY AT CENTER OF GRAVITY AND 0.90c. VEHICLE WITH ACTIVE SUSPENSION

The accelerations at the c.g. are greatly improved over the rigid vehicle (0.121g) and somewhat better than the passive suspension (0.007lg) having a rms value of 0.002lg. This corresponds to a very smooth and comfortable ride as shown by comparison of the rms vertical acceleration with the ISO Specification in Figure 12. The vehicle acceleration response is about two decades below the specifications. The acceleration at the rearmost seat is even smaller, being on the order of 0.001g. The seats in between will have values ranging between these two, so that, the overall level of vertical acceleration is very low.

The rms gap variation is on the order of one-third inch, that being the criterion used in the cost function. There is a tradeoff between gap variation and acceleration, and the cost function was adjusted until this level of gap variation was met but not exceeded. Hence the gap values of 0.218 inch at the leading edge and 0.327 inch at the trailing edge are not so much a result of the analysis as they are one of the design conditions for the active controller. These values imply that the steady-state gap is greater than three standard deviations on the normal distribution, implying that contact is rare. As with the passive suspension, there is a reversal from the rigid case in the relative size of leading and trailing edge gap variation.

The typical winglet motions are slightly larger for the active controller; the rms $\Delta\delta_{w_1}$ is 0.025 rad. which corresponds to 0.75 inch at the tip, and rms $\Delta\delta_{w_2}$ is 0.00055 rad. corresponding to a trailing edge gap variation of 0.594 inch. These are both significant motions with regard to the size of the gap, but they are small enough on the vehicle level to imply that the power required for the winglets is likely to be relatively

performance is still considerably better than the rigid vehicle. With only the relative height and pitch displacement feedbacks, the rms accelerations increase to 0.017g at the c.g. (0.40c) and 0.026g at the trailing edge (0.90c). While larger than the complete system values, they still constitute a smooth ride. The respective spectral densities are shown in Figure 13. Figure 14 shows a comparison of the rms vertical acceleration with the ISO Specification indicating that although there is increased vehicle response the ISO Specification is met. The indication of this investigation is that attitude feedback is most crucial, while rate feedback fine-tunes the response and adds some degree of smoothness. Guideway shape feedback is unnecessary.

Overall, the active control does an extremely effective job of smoothing out the ride and maintaining a reasonable gap clearance. The acceleration levels are somewhat improved over the passive suspension, though there might be reasonable doubt that the improvement is worth the extra cost of the active system over the passive. The active controller does, however, yield accelerations on the order of 0.002g or less (depending on position inside the passenger compartment), and requires very small control deflections and hence small control power, and permits selection of the levels of gap variation of the vehicle by adjusting the weighting in the cost function. The feedback gains are small and therefore easily realized. In addition, the active system provides insight into the limits of vehicle performance. It seems that, as a result of this analysis, the ride qualities of the TRACV at its best seems to be very promising indeed.

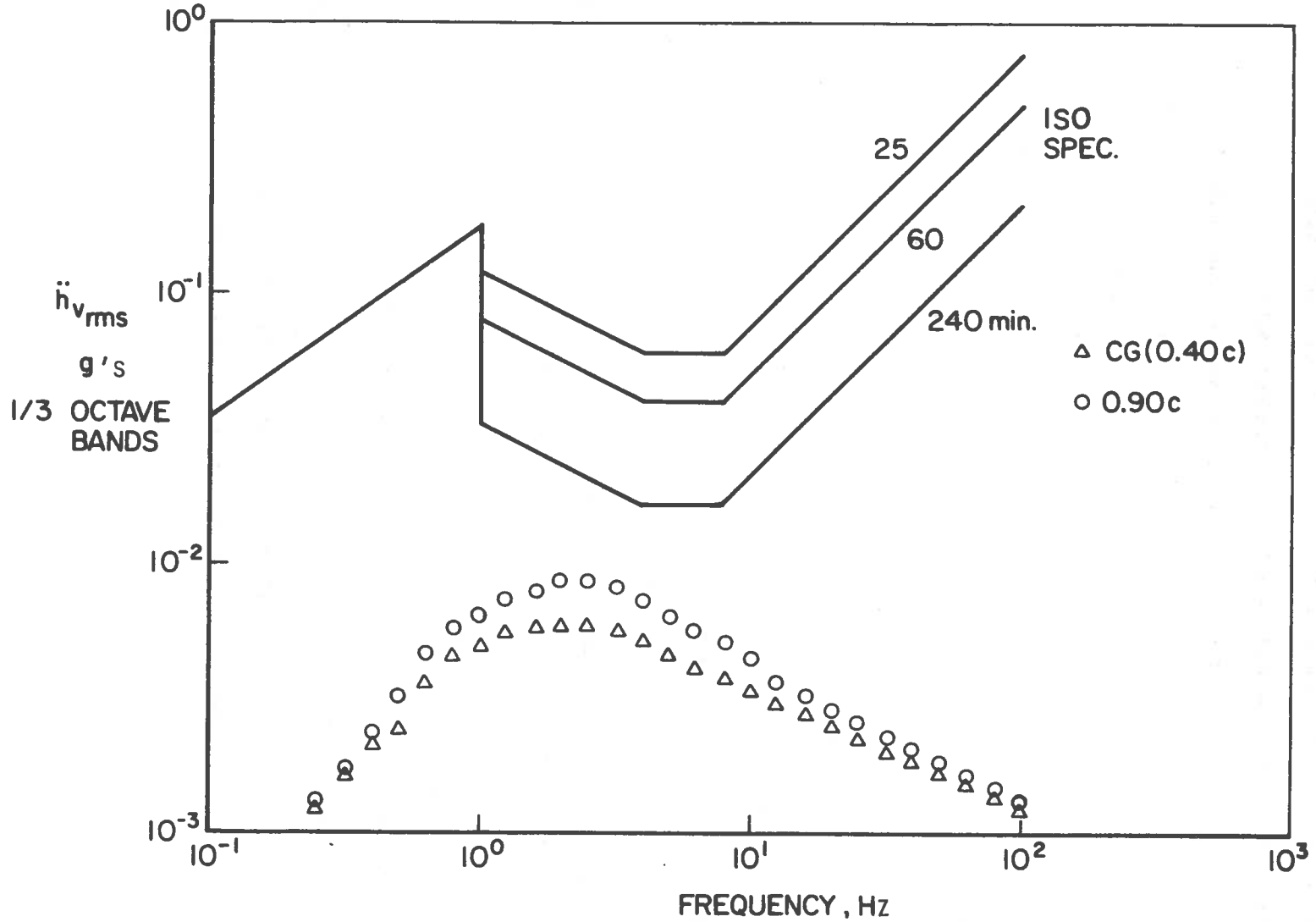

FIGURE 14. COMPARISON OF RMS VERTICAL ACCELERATION IN ONE-THIRD OCTAVE BANDS WITH ISO SPECIFICATIONS. VEHICLE WITH PARTIALLY BLIND ACTIVE SUSPENSION

sensitive especially to the two feedback paths $\bar{h}_r \rightarrow \Delta\delta_{w_1}$ and $\theta_r \rightarrow \Delta\delta_{w_2}$ both of which act to reduce markedly the natural frequencies and if either of these gains increases there will be a tendency towards vehicle instability. It would therefore be highly desirable to conduct a sensitivity study of this feedback system.

Since the passive controller fundamentally operates in a different fashion it would not be expected to suffer from this sensitivity.

5. CONCLUSIONS

The longitudinal dynamic modes of motion of a Tracked Ram Air Cushion Vehicle exhibit a considerable degree of pitch-heave coupling. The rigid vehicle modes of motion are characterized by two comparatively high frequency oscillatory modes with low inherent damping. As a consequence of the high frequencies and low damping, the vertical accelerations experienced in the passenger compartment, for a vehicle operating in a guideway with a roughness level typical of modern highways, exceed the ISO standards for the comfortable ride. Further, analysis of rigid vehicle motion amplitudes indicated that it would frequently contact the guideway.

Therefore, various suspension system designs were studied with the aim of improving the ride qualities. Basically two alternative suspension system designs were examined, a passive system and an active system.

The passive suspension system consisted of providing two degrees of freedom of winglet motion with respect to the body of the vehicle and placing springs and dampers about the rotation axes to improve the ride qualities. It was found that by suitable selection of the spring and damper characteristics a very comfortable ride with vertical accelerations well below the ISO ride comfort standard could be achieved. Further the study indicates that with this suspension system, guideway contact would be rare. Essentially the winglet follows the guideway irregularities and the body exhibits very little response to the guideway.

The use of an active control system, designed by optimal control techniques, where motions of the vehicle and guideway shape are sensed and employed to move the winglets with respect to the body results in a very

as a function of wave length may give different results for the prediction of the rigid vehicle response characteristics. This approximation is probably less significant for the vehicle with the active and passive suspension systems since the natural frequencies of the vehicle are reduced, however, it should be recalled that if no approximation is made with respect to the influence of guideway disturbances, an infinite rms acceleration will be predicted.

It would also be of interest to examine alternate methods of providing control for a TRACV. A two-degree-of-freedom winglet is difficult to mechanize unless at least one of the two degress of freedom is provided through elastic flexibility.

Ribich, W. A., Captain, K. M. and Richardson, H. H.: "An Analysis of the Effects of Finite Fluid-Suspension Pad Length on the Dynamics of a Vehicle on an Irregular Guideway", MIT Engineering Projects Laboratory Report No. DSR-76110-6, September 1967.

Schultz, D. G. and Melsa, J. L.: STATE FUNCTIONS AND LINEAR CONTROL SYSTEMS, McGraw-Hill Book Company, New York, 1967.

APPENDIX A

EQUATIONS OF MOTION

The dynamic model of the TRACV employed in this study involves two-degrees-of-freedom, heave and pitch. It is assumed that the horizontal velocity is constant. There is no longitudinal/lateral coupling as a result of the symmetry of the vehicle and the linearized approach. Consequently only the lift and pitching moment equations are developed. The aerodynamic lift and pitching moment are expanded in a Taylor series about the equilibrium flight condition. Thus the lift and pitching moment can be expressed as the sum of an equilibrium or steady-state term and a perturbation, $L = L_o + (\Delta L)_A$ where

$$(\Delta L)_A = + \frac{\partial L}{\partial \dot{h}_r} \Delta \dot{h}_r + \frac{\partial L}{\partial \dot{\theta}_r} \Delta \dot{\theta}_r + \frac{\partial L}{\partial h_r} \Delta h_r + \frac{\partial L}{\partial \theta_r} \Delta \theta_r$$

and $M = M_o + (\Delta M)_A$ where (A-1)

$$(\Delta M)_A = + \frac{\partial M}{\partial \dot{h}_r} \Delta \dot{h}_r + \frac{\partial M}{\partial \dot{\theta}_r} \Delta \dot{\theta}_r + \frac{\partial M}{\partial h_r} \Delta h_r + \frac{\partial L}{\partial \theta_r} \Delta \theta_r$$

The steady-state equilibrium condition is given by

$$L_o = mg$$

$$M_o = 0 \quad . \tag{A-2}$$

Winglet motion is considered as a control input. Two winglet deflections, are included, rotation about the longitudinal axis of the yehicle, δ_{w_1} and rotation about the lateral axis δ_{w_2}. Only symmetric motions of the

The term $\left[\frac{c\ C_{L_o}}{g}\right]$ has the units sec^2, and is therefore used to define a time scale for the dynamic motion. Define,

$$\tau_D = \left[\frac{c\ C_{L_o}}{g}\right]^{\frac{1}{2}} \tag{A-5}$$

Equation (A-4) can be written as

$$\tau_D^2\ \ddot{\bar{h}}_V = \Delta C_L \tag{A-6}$$

The time is nondimensionalized in the equation of motion (A-6) and the notation $()'$ is used to indicate differentiation with respect to dimensionless time, i.e.,

$$\bar{h}_V'' = \frac{d^2\ \bar{h}}{d\ (\frac{t}{\tau_D})^2} = \tau_D^2\ \ddot{\bar{h}}_V$$

Consequently, equation (A-6) can be written as

$$\bar{h}_V'' = \Delta C_L \tag{A-7}$$

As noted in Appendix B a different time scale, τ_A, arises in the development of the aerodynamic derivatives. The relationship between the time derivatives in the two systems is

$$D\bar{h} = \frac{\tau_A}{\tau_D}\ \bar{h}' \qquad D\theta = \frac{\tau_A}{\tau_D}\ \theta'$$

The ratio of the two time scales can be expressed in terms of the relative density of the vehicle, μ, where

$$\mu = \frac{m}{\rho S c}$$

$$+ \begin{bmatrix} C_{L_{\bar{h}}} & C_{L_\theta} \\ C_{M_{\bar{h}}} & C_{M_\theta} \end{bmatrix} \begin{Bmatrix} \bar{h}_r \\ \theta_r \end{Bmatrix} + \begin{bmatrix} C_{L_{\delta_{w_1}}} & C_{L_{\delta_{w_2}}} \\ C_{M_{\delta_{w_1}}} & C_{M_{\delta_{w_2}}} \end{bmatrix} \begin{Bmatrix} \delta_{w_1} \\ \delta_{w_2} \end{Bmatrix} \tag{A-10}$$

It should be noted that the aerodynamic derivatives produce forces as a function of motion relative to the guideway. Consequently, to complete the description of the vehicle motion, the shape of the guideway with respect to an inertial reference must be included. h_g is defined as the height of the guideway above the inertial reference, and θ_g is the slope of the guideway with respect to the reference plane as shown in Figure 1. Therefore, the relationship required for the displacements are,

$$\begin{aligned} \bar{h}_r &= \bar{h}_v - \bar{h}_g \\ \theta_r &= \theta_v - \theta_g \end{aligned} \tag{A-11}$$

Since the guideway irregularity is a function of horizontal distance, x, as the vehicle moves over the guideway at a velocity, U, the vehicle will experience inputs from the guideway which depend upon time. That is, since

$$\begin{aligned} h_g &= h_g(x) \\ \theta_g &= \theta_g(x) \end{aligned} \tag{A-12}$$

Therefore

$$\begin{aligned} \dot{h}_g &= \frac{dh_g}{dx} \frac{dx}{dt} = U \frac{dh_g}{dx} \\ \dot{\theta}_g &= \frac{d\theta_g}{dx} \frac{dx}{dt} = U \frac{d\theta_g}{dx} \end{aligned} \tag{A-13}$$

In addition, by the definition of θ_g and h_g, when θ_g is small

$$\theta_g = \frac{dh_g}{dx} \tag{A-14}$$

where

$$x_v = \begin{Bmatrix} \bar{h}_v \\ \theta_v \end{Bmatrix}$$

$$x_g = \begin{Bmatrix} \bar{h}_g \\ \theta_g \end{Bmatrix}$$

$$u = \begin{Bmatrix} \delta_{w_1} \\ \delta_{w_2} \end{Bmatrix} .$$

The variables describing the guideway shape are related by

$$\bar{h}'_g = (2\mu)^{\frac{1}{2}} \theta_g \quad .$$

The elements of the matrices are given in Table D-1.

Elsewhere in the report equations (A-18) are converted to state vector form for convenience in making numerical calculations.

For this analysis, the steady-state lift coefficient is taken to be $C_{L_o} = 0.455$ at a forward velocity of 300 fps. For the assumed vehicle geometry, the gross weight for equilibrium is 110,000 lbs., corresponding closely to the vehicle studied by Fraize and Barrows (1973). Also the present model implies $\tau_p = 1.456$ sec. It should be noted that no upper surface contribution to lift or moment is included. In actuality, the shape described adds a $\Delta C_L \cong 0.25$, which will slightly alter the trim conditions if included.

APPENDIX B

STABILITY DERIVATIVES

Theoretical expressions for the displacement and rate dependent stability derivatives are presented in this appendix. The derivation of the displacement derivatives is presented in Curtiss and Putman (1977). The rate derivatives were developed based on quasi-static aerodynamic theory (the reduced frequency $\hat{\omega}$ is assumed to be small). Incompressible flow is assumed and the expressions given below have been linearized about zero pitch attitude. The natural time scale for nondimensionalization of the rate derivatives is $\tau_A = \frac{c}{U}$ and dimensionless rates are denoted by D(), that is,

$$Dh = \frac{dh}{d(\frac{t}{\tau_A})} = \frac{c}{U}\dot{h}$$

$$D\theta = \frac{d\theta}{d(\frac{t}{\tau_A})} = \frac{c}{U}\dot{\theta} \qquad \text{(B-1)}$$

It should be noted that a different time scale is convenient for the dynamic equations of motion. The displacement derivatives are

$$\frac{\partial C_L}{\partial \bar{h}} = \frac{-\bar{\alpha}^2}{\alpha_o}\frac{\partial C_L}{\partial \bar{\alpha}} + \frac{2c}{\alpha_o \bar{W}}\frac{\partial C_L}{\partial r_o}$$

$$\frac{\partial C_L}{\partial \theta} = \frac{1}{\alpha_o}\left\{[\bar{\alpha} + \bar{\alpha}^2(1 - \bar{x}_o)]\frac{\partial C_L}{\partial \bar{\alpha}} - r_o\frac{\partial C_L}{\partial r_o} - \frac{2c}{W}\frac{\partial C_L}{\partial r_1}\right\}$$

$$\frac{\partial C_M}{\partial \bar{h}} = \frac{-\bar{\alpha}^2}{\alpha_o}\frac{\partial C_M}{\partial \bar{\alpha}} + \frac{2c}{\alpha_o \bar{W}}\frac{\partial C_M}{\partial r_o} \qquad \text{(B-2)}$$

$$\frac{\partial C_M}{\partial \theta} = \frac{1}{\alpha_o}\left\{[\bar{\alpha} + \bar{\alpha}^2(1 - \bar{x}_o)]\frac{\partial C_M}{\partial \bar{\alpha}} - r_o\frac{\partial C_M}{\partial r_o} - \frac{2c}{W}\frac{\partial C_M}{\partial r_1}\right\}$$

moment coefficient:

$$\frac{\partial C_L}{\partial \delta_{w_1}} = \frac{\partial C_L}{\partial r_o} \cdot \frac{\partial r_o}{\partial \delta_{w_1}} = \frac{\partial C_L}{\partial r_o} \left(\frac{0.707\ W_w}{W\ \alpha} \right)$$

$$\frac{\partial C_M}{\partial \delta_{w_1}} = \frac{\partial C_M}{\partial r_o} \cdot \frac{\partial r_o}{\partial \delta_{w_1}} = \frac{\partial C_M}{\partial r_o} \left(\frac{0.707\ W_w}{W\ \alpha} \right) . \qquad \text{(B-5)}$$

In general, rotation of the winglet about the lateral axis of the vehicle about the point $\bar{x}_{cr}$ will change both r_o and r_1.

$$\Delta r_o = \frac{2\,c}{W\,\alpha} \left(\bar{x}_{cr} - \bar{x}_{cg} \right) \Delta \delta_{w_2}$$

$$\Delta r_1 = - \frac{2\,c}{W\,\alpha} \Delta \delta_{w_2} \qquad \text{(B-6)}$$

Winglet rotation about the vehicle center of gravity ($\bar{x}_{cg}$) is considered, so that the change in lift and pitching moment coefficient due to winglet rotation $\Delta \delta_{w_2}$ are

$$\frac{\partial C_L}{\partial \delta_{w_2}} = \frac{\partial C_L}{\partial r_1} \cdot \frac{\partial r_1}{\partial \delta_{w_2}} = \frac{\partial C_L}{\partial r_1} \left(- \frac{2\,c}{W\,\alpha} \right)$$

$$\frac{\partial C_M}{\partial \delta_{w_2}} = \frac{\partial C_M}{\partial r_1} \left(- \frac{2\,c}{W\,\alpha} \right) \qquad \text{(B-7)}$$

Recall that the subscript notation in the case of the pitching moment coefficient incorporates the radius of gyration,

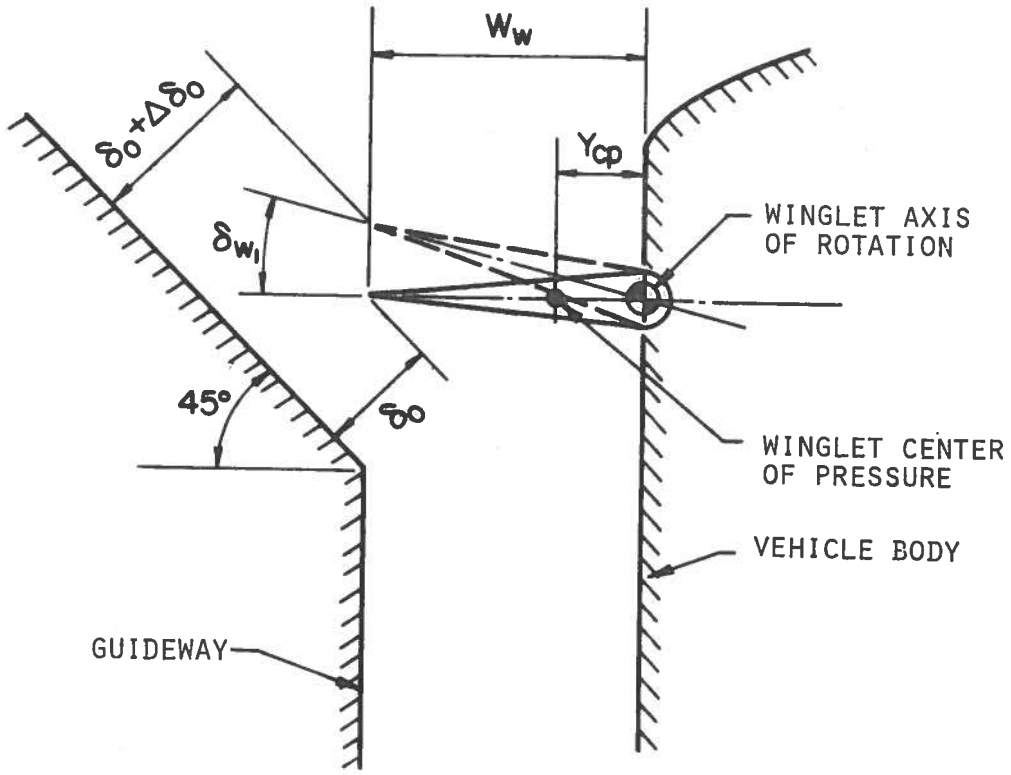

FIGURE B-1. GEOMETRY OF THE PERTURBED WINGLET

APPENDIX C

GUIDEWAY DISTURBANCE DESCRIPTION

a.) Finite Pad Length Effect

As a TRACV vehicle travels over a guideway, surface irregularities of the guideway will alter the aerodynamic forces acting on the vehicle. Since the irregularities occur at all wavelengths, some of the irregularities will be of much shorter wavelength than the length of the vehicle. When this is the case, the shape of the ground with respect to the vehicle cannot be described by the displacement at a single point, as is the case with a point contact suspension, but instead the aerodynamic model must include an irregular shape along the length of the vehicle. To a point contact suspension, a stairstep in the guideway is a step change in surface height, but to a pad of finite length it is an obstacle to be climbed. A step change in surface height implies that all points under the pad change height simultaneously with the aerodynamic model employed.

The aerodynamic model of the TRACV employed here is a lumped parameter model, that is, stability derivatives express the forces and moment acting on the vehicle in terms of vehicle height and attitude with respect to the guideway, effectively assuming that the wavelength of guideway irregularities is long compared to the length of the vehicle implying that the variation of guideway shape is linear along the length of the vehicle. Further, the rate dependent aerodynamics were developed using quasi-steady theory, that is, the reduced frequency is assumed to be small which is equivalent to assuming that the wavelength of the guideway irregularities is long compared to vehicle length. Consequently, a typical surface spectrum applied as an

$$\bar{h}_g = |\bar{h}_g(\lambda)| \cos\left(\frac{2\pi}{\lambda}(x + Ut)\right)$$

where x is measured from the center of the vehicle. Normalizing the guideway amplitude to one, and expressing the nondimensional height in terms of reduced frequency and nondimensional aerodynamic time

$$\bar{h}_g = \cos\left[\hat{\omega}\ (\bar{x} + \hat{t})\right]$$

The average height under the vehicle is

$$\hat{h}_{g_{avg}} = \int_{-\frac{1}{2}}^{\frac{1}{2}} \cos\left[\hat{\omega}\ (\bar{x} + \hat{t})\right] d\bar{x} \ .$$

Consequently,

$$\bar{h}_{g_{avg}} = \left(\frac{2}{\hat{\omega}} \sin\frac{\hat{\omega}}{2}\right) \cos\hat{\omega}\ \hat{t} \ . \qquad \text{(C-1)}$$

The function in parentheses is plotted in Figure C-1 showing that it approaches zero as the reduced frequency (or chord to wavelength ratio) increases resulting in an attenuation which will result in a finite vehicle rms acceleration when applied as an input to the vehicle.

Similarly, the average velocity is

$$D\bar{h}_{g_{avg}} = \left(2 \sin\frac{\hat{\omega}}{2}\right) \sin\hat{\omega}\ \hat{t} \ . \qquad \text{(C-2)}$$

The slope of the guideway is related to the height by the following equation,

$$\theta_g = \frac{\dot{h}_g}{U} = D\bar{h}_g$$

that is

$$\theta_{g_{avg}} = \left(2 \sin\frac{\hat{\omega}}{2}\right) \sin\hat{\omega}\ \hat{t} \qquad \text{(C-3)}$$

Similarly,

$$D\theta_{g_{avg}} = (2\,\hat{\omega}\,\sin\frac{\hat{\omega}}{2})\cos\hat{\omega}\,\hat{t}\,. \qquad \text{(C-4)}$$

Thus, the effect of using average guideway parameters is to add attenuation to the guideway input to the vehicle as a function of reduced frequency. Consequently, this effect is added to the dynamic model. It is possible and convenient to approximate the function $|\frac{2}{\hat{\omega}}\sin\frac{\hat{\omega}}{2}|$ by a linear second order filter. Using a linear filter has the advantage that it can be simply incorporated into the dynamic model. A second order filter assures that the vehicle will not experience infinite rms accelerations. Figure C-1 shows the magnitude of the frequency response function

$$G_p(i\,\hat{\omega}) = \frac{1}{(1 + 0.24\,i\,\hat{\omega})(1 + 0.36\,i\,\hat{\omega})} \qquad \text{(C-5)}$$

which is used to approximate the more complex attenuation function given by equation (C-1).

b.) Guideway Roughness Description

In order to represent the guideway roughness as a disturbance to the vehicle, the following approach is taken. Experimental data indicate that a reasonable model of the vertical roughness of a roadway can be represented by the following power spectral density (Hedrick, Billington and Dreesbach, 1974):

$$\Phi_{h_g}(\Omega) = \frac{A}{\Omega^2} \qquad \text{(C-6)}$$

The power spectrum of the slope of the guideway can be obtained from equation (C-8) noting that

$$\frac{dx}{dt} = U \, .$$

Consequently

$$\frac{1}{U} \dot{h}_g = \theta_g \, . \tag{C-12}$$

It is convenient to view the input spectrum given by equation (C-11) as produced by white noise input which has passed through a linear filter. Consider a filter with a transfer function G_1 with an input $\Phi_n(\omega)$ (white noise) and an output $\Phi_{h_g}(\omega)$ as given above.

The relationship between the input and the output is given by

$$\Phi_{h_g}(\omega) = |G_1|^2 \, \Phi_n(\omega) \tag{C-13}$$

Now, $\Phi_{h_g}(\omega)$ is given by equation (C-11) as

$$\Phi h_g(\omega) = \frac{AU}{\omega^2} \tag{C-11}$$

It is convenient to nondimensionalize the right hand side of equation (C-11) using the dynamic time scale such that,

$$\tilde{\Phi}_{\tilde{h}_g}(\tilde{\omega}) = \frac{\tau_D}{\tau_A} \left[\frac{\bar{A}}{(\tilde{\omega})^2}\right] = \frac{(2\mu)^{\frac{1}{2}} \bar{A}}{(\tilde{\omega})^2} \tag{C-14}$$

The power spectral density given by equation (C-14) can be expressed in terms of a dimensionless white noise input, $\bar{\eta}(\tilde{t})$, with a unity spectral density ($\tilde{\Phi}_{\bar{n}}(\tilde{\omega}) = 1$) which has been passed through a filter whose characteristic

Thus, to summarize

$$\frac{\bar{h}_{ga}(\tilde{s})}{\bar{h}_{g}(\tilde{s})} = G_p(\tilde{s}) , \qquad \frac{\bar{h}_{g}(\tilde{s})}{\bar{\eta}(\tilde{s})} = G_1(\tilde{s}) . \tag{C-19}$$

The apparent guideway slope $\theta_{ga}(\tilde{s})$ is related to $\bar{h}_{ga}(\tilde{s})$ by equation (C-16). Thus the second order filter represented by equation (C-17) can be inserted after the element representing the guideway spectrum as shown in Figure 3. This final block diagram represents the manner in which the inputs disturb the vehicle. This organization of the input spectrum is convenient since it is now possible to view the input to the system as white noise making it convenient to apply optimal control techniques. That is, the guideway characteristics are represented as a set of coupled ordinary linear differential equations with a white noise input. From the final block diagram in Figure 3, the guideway equations can be written in the dimensionless dynamic time domain as

$$\begin{aligned} \theta''_{ga} + 9.82\ (\mu)^{\frac{1}{2}}\ \theta'_{ga} + 23.15\ \mu\ \theta_{ga} &= 19.46\ \mu^{3/4}\ \bar{A}^{\frac{1}{2}}\ \bar{\eta}(t) \\ \bar{h}'_{ga} &= (2\mu)^{\frac{1}{2}}\ \theta_{ga} . \end{aligned} \tag{C-20}$$

These equations are part of the complete system model. These two equations represent a good approximation to a function which results from assuming that the parameters which determine the response of the TRACV to guideway roughness are the average height and slope of the guideway under the vehicle at a given point in time. They have been arranged so that

APPENDIX D

STATE MATRIX FORM

The most convenient way to express the complete system equations of motion is in state matrix form. Appendix A gives the vehicle equations of motion (equation A-18) as

$$x_v'' + C\,x_v' + K\,x_v = C\,x_g' + K\,x_g + F\,u \qquad \text{(D-1)}$$

where

$$x_v = \begin{Bmatrix} \bar{h}_v \\ \theta_v \end{Bmatrix}$$

$$x_g = \begin{Bmatrix} \bar{h}_{ga} \\ \theta_{ga} \end{Bmatrix}$$

$$u = \begin{Bmatrix} \delta_{w_1} \\ \delta_{w_2} \end{Bmatrix} .$$

Equations (A-11) relate the relative coordinates to the absolute coorinates, and can be written in the above notation as

$$x_r = x_v - x_g \qquad \text{(D-2)}$$

The guideway equations given by equations (C-20) can be expressed in matrix form as

$$A_2\,x_g'' + A_1\,x_g' + A_o\,x_g = B_o\,\bar{\eta}(\tilde{t}) . \qquad \text{(D-3)}$$

The equations of motion are

$$\{x'\} = \begin{bmatrix} -C & -K & C & 0 \\ I & 0 & -I & 0 \\ 0 & 0 & -\tilde{A}_1 & -\tilde{A}_2 \\ 0 & 0 & 0 & 1 \end{bmatrix} \{x\} + \begin{bmatrix} F \\ 0 \\ 0 \\ 0 \end{bmatrix} \{u\} + \begin{bmatrix} 0 \\ 0 \\ B_o \\ 0 \end{bmatrix} \{\bar{\eta}(\tilde{t})\} \qquad \text{(D-9)}$$

where I is a unit matrix. In compact notation,

$$x' = A\,x + B\,u + D\,w \qquad \text{(D-10)}$$

For the rigid vehicle, u = 0. The matrices A, B and C are given in Table D-II in literal form and in Table D-III in numerical form as employed in this analysis

$$u = \begin{Bmatrix} \Delta\delta_{w_1} \\ \Delta\delta_{w_2} \end{Bmatrix} \qquad \text{and} \qquad w = \{\bar{\eta}(\tilde{t})\} .$$

For the passive suspension case, the winglet deflections $\Delta\delta_{w_1}$ and $\Delta\delta_{w_2}$ are taken to be state variables ($u = x_w$). The equations of motion for the free winglets are given by equations (20) and can be written in matrix notation as

$$x_w' = H_1\,x_r' + H_2\,x_r + H_3\,x_w \qquad \text{(D-11)}$$

the leading and trailing edge gap variations and the two control deflections. Denoting by y the vector of quantities to be weighted

$$y = \begin{Bmatrix} \ddot{h}_v \\ \ddot{\theta}_v \\ \delta_{LE} \\ \delta_{TE} \\ \delta_{w_1} \\ \delta_{w_2} \end{Bmatrix}$$

y can be related to the state variables and the control variables by the following matrix equation

$$y = M \begin{bmatrix} x \\ u \end{bmatrix}$$

where x is given in dimensionless terms by equation (D-4) so that

$$\begin{bmatrix} x \\ u \end{bmatrix} = \begin{Bmatrix} \dot{h}_v \\ \dot{\theta}_v \\ h_r \\ \theta_r \\ \dot{h}_{ga} \\ \dot{\theta}_{ga} \\ \theta_{ga} \\ \Delta\delta_{w_1} \\ \Delta\delta_{w_2} \end{Bmatrix}$$

TABLE D-I

MATRIX ELEMENTS IN EQUATIONS OF MOTION

$$C = \frac{1}{(2\mu)^{\frac{1}{2}}} \begin{bmatrix} -C_{L_{D\bar{h}}} & -C_{L_{D\theta}} \\ -C_{M_{D\bar{h}}} & -C_{M_{D\theta}} \end{bmatrix}$$

$$K = \begin{bmatrix} -C_{L_{\bar{h}}} & -C_{L_{\theta}} \\ -C_{M_{\bar{h}}} & -C_{M_{\theta}} \end{bmatrix}$$

$$F = \begin{bmatrix} C_{L_{\delta_{w_1}}} & C_{L_{\delta_{w_2}}} \\ C_{M_{\delta_{w_1}}} & C_{M_{\delta_{w_2}}} \end{bmatrix}$$

$$A_2 = \begin{bmatrix} 0 & 0 \\ 0 & 1 \end{bmatrix}$$

$$A_1 = \begin{bmatrix} 1 & 0 \\ 0 & 9.82(\mu)^{\frac{1}{2}} \end{bmatrix}$$

TABLE D-I

MATRIX ELEMENTS IN EQUATIONS OF MOTION (Cont.)

$$H_1 = \begin{bmatrix} \frac{h_m \bar{y}_{cp}}{b_1 (2\mu)^{\frac{1}{2}}} C_{L_{Dh}} & \frac{h_m \bar{y}_{cp}}{b_1 (2\mu)^{\frac{1}{2}}} C_{L_{D\theta}} \\ \frac{h_m \bar{k}_y^2}{b_2 (2\mu)^{\frac{1}{2}}} C_{M_{D\bar{h}}} & \frac{h_m \bar{k}_y^2}{b_2 (2\mu)^{\frac{1}{2}}} C_{M_{D\theta}} \end{bmatrix}$$

$$H_2 = \begin{bmatrix} \frac{h_m \bar{y}_{cp}}{b_1} C_{L_{\bar{h}}} & \frac{h_m \bar{y}_{cp}}{b_1} C_{L_\theta} \\ \frac{h_m \bar{k}_y^2}{b_1} C_{M_{\bar{h}}} & \frac{h_m \bar{k}_y^2}{b_1} C_{M_\theta} \end{bmatrix}$$

$$H_3 = \begin{bmatrix} \frac{h_m \bar{y}_{cp} C_{L_{\delta_{w_1}}} - K_1}{b_1} & \frac{h_m \bar{y}_{cp} C_{L_{\delta_{w_2}}}}{b_1} \\ \frac{h_m \bar{k}_y^2 C_{M_{\delta_{w_1}}}}{b_1} & \frac{h_m \bar{k}_y^2 C_{M_{\delta_{w_2}}} - K_2}{b_1} \end{bmatrix}$$

TABLE D-II

RIGID VEHICLE EQUATIONS OF MOTION IN STATE VECTOR FORM

$$(x' = Ax + Dw)$$

$$A = \begin{bmatrix}
\frac{1}{(2\mu)^{\frac{1}{2}}} C_{L_{D\bar{h}}} & \frac{1}{(2\mu)^{\frac{1}{2}}} C_{L_{D\theta}} & C_{L_{\bar{h}}} & C_{L_{\theta}} & -\frac{1}{(2\mu)^{\frac{1}{2}}} C_{L_{D\bar{h}}} & -\frac{1}{(2\mu)^{\frac{1}{2}}} C_{L_{D\theta}} & 0 \\
\frac{1}{(2\mu)^{\frac{1}{2}}} C_{M_{D\bar{h}}} & \frac{1}{(2\mu)^{\frac{1}{2}}} C_{M_{D\theta}} & C_{M_{\bar{h}}} & C_{M_{\theta}} & -\frac{1}{(2\mu)^{\frac{1}{2}}} C_{M_{Dh}} & -\frac{1}{(2\mu)^{\frac{1}{2}}} C_{M_{D\theta}} & 0 \\
1 & 0 & 0 & 0 & -1 & 0 & 0 \\
0 & 1 & 0 & 0 & 0 & -1 & 0 \\
0 & 0 & 0 & 0 & 0 & (2\mu)^{\frac{1}{2}} & 0 \\
0 & 0 & 0 & 0 & 0 & -1.67(2\mu)^{\frac{1}{2}} & 11.57(2\mu) \\
0 & 0 & 0 & 0 & 0 & 1 & 0
\end{bmatrix}$$

$$D = \begin{bmatrix} 0 \\ 0 \\ 0 \\ 0 \\ 0 \\ (11.57)(2\mu)^{3/4}\ \bar{A}^{\frac{1}{2}} \end{bmatrix}$$

TABLE D-IV

TRANSFORMATION MATRIX FOR COST FUNCTION VARIABLES

$$M = \begin{bmatrix}
\frac{1}{(2\mu)^{\frac{1}{2}}} C_{L_{D\bar{h}}} & \frac{1}{(2\mu)^{\frac{1}{2}}} C_{L_{D\theta}} & C_{L_{\bar{h}}} & C_{L_{\theta}} & -\frac{1}{(2\mu)^{\frac{1}{2}}} C_{L_{D\bar{h}}} & -\frac{1}{(2\mu)^{\frac{1}{2}}} C_{L_{D\theta}} & 0 & C_{L_{\delta_{w_1}}} & C_{L_{\delta_{w_2}}} \\
\frac{1}{(2\mu)^{\frac{1}{2}}} C_{M_{D\bar{h}}} & \frac{1}{(2\mu)^{\frac{1}{2}}} C_{M_{D\theta}} & C_{M_{\bar{h}}} & C_{M_{\theta}} & -\frac{1}{(2\mu)^{\frac{1}{2}}} C_{M_{D\bar{h}}} & -\frac{1}{(2\mu)^{\frac{1}{2}}} C_{M_{D\theta}} & 0 & C_{M_{\delta_{w_1}}} & C_{M_{\delta_{w_2}}} \\
0 & 0 & 1 & \bar{x}_{cg} & 0 & 0 & 0 & 0 & \bar{x}_{cg} \\
0 & 0 & 1 & -(1-\bar{x}_{cg}) & 0 & 0 & 0 & 0 & -(1-\bar{x}_{cg}) \\
0 & 0 & 0 & 0 & 0 & 0 & 0 & 1 & 0 \\
0 & 0 & 0 & 0 & 0 & 0 & 0 & 0 & 1
\end{bmatrix}$$

APPENDIX E

OPTIMIZATION SOLUTION FORMAT

The optimization of the passive and active suspensions was implemented on the digital computer using the interactive language known as APL. The two techniques varied somewhat from one another. Figure E-1 shows the logic flow for the passive case, Figure E-2 depicts the flow for the active case.

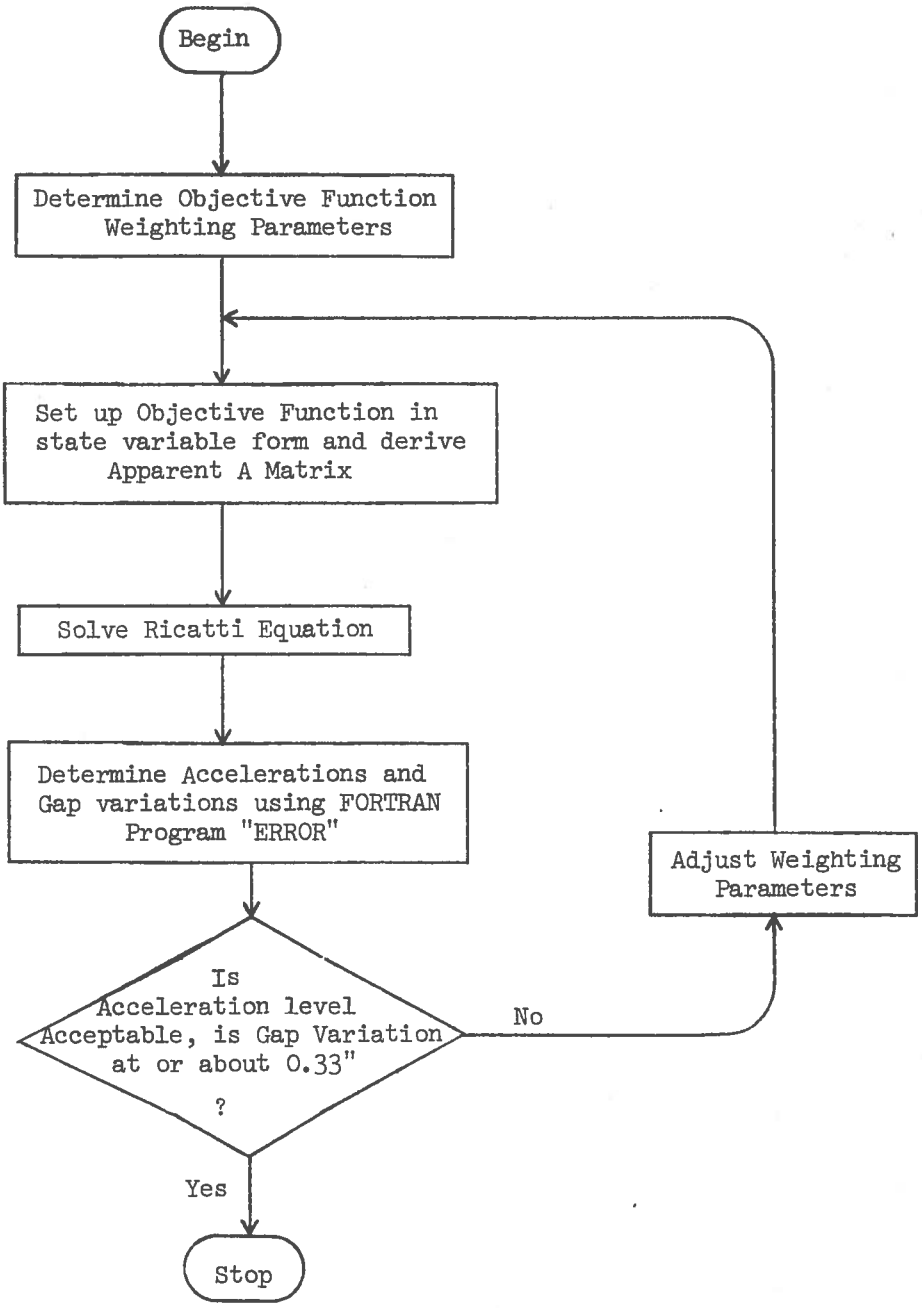

FIGURE E-2. ACTIVE CONTROL SOLUTION TECHNIQUE

APPENDIX F

REPORT OF NEW TECHNOLOGY

After diligent review of the work performed under this contract, no innovation, discovery, improvement, or invention of a patentable nature was made. The unconventional vehicle configuration which is described herein originated from previous efforts. The main contribution of the present report is to obtain an improved understanding of the dynamic performance of the vehicle.

110 Copies